MOTION SYNCHRONIZATION OF MULTIPLE PIEZOELECTRIC ACTUATORS (PEAS) USING THE LINEAR ACTIVE DISTURBANCE REJECTION CONTROLLER (LADRC)

GANESH RAMKUMAR

A THESIS SUBMITTED TO THE FACULTY OF GRADUATE STUDIES
IN PARTIAL FULFILMENT OF THE REQUIREMENTS
FOR THE DEGREE OF
MASTER OF SCIENCE

GRADUATE PROGRAM IN EARTH AND SPACE SCIENCE
YORK UNIVERSITY
TORONTO, ONTARIO
DECEMBER 2018

Abstract

This thesis investigates how the Linear Active Disturbance Rejection Controller (LADRC) can be used with the synchronous strategy for motion synchronization of multiple piezoelectric actuators (PEAs). Both a single PEA system and a three PEA system are used to validate the control system. The investigation consists of a brief introduction of the LADRC, system identification of a single PEA and three PEA system, parameter estimation of the LADRC, implementation of the LADRC for a single PEA and for a three PEA system with the synchronization strategy, a comparison between the LADRC using the synchronization strategy and Linear Quadratic Gaussian (LQG) using the synchronization strategy. The investigation demonstrated that the synchronized LADRC is a viable and simple control solution for the three PEA system, used to control the gap spacing between the mirrors of the Fabry - Peŕot Spectrometer flown by SDCNLab in stratospheric balloon missions.

Acknowledgments

I would like to first of all thank Professor Jinjun Shan for inspiring me during my bachelors degree to purse a Master's degree and then for taking me on as his Master's student. With his help I was able to participate in the 2017 Alice Springs Balloon Launch and help launch SDCNLab's Fabry Pérot spectrometer on a balloon to the stratosphere. It was an enjoyable and learning experience and a great opportunity to make memories. Furthermore, he helped me get two internships at Microsat Systems Canada Inc., where I was able to experience the life in industry as a Space engineer. He was also the one who motivated me to research the LADRC and the synchronization scheme, which is the essence of my thesis.

Throughout my experience at the SDCNLab I have met many people and built many connections. To everyone I met in the lab Mike, Marc, Mohammed, Scott, Ali, Hassan, Samira, Dr. Ren, Dr. Ti Chen, Dr. Ja, Dr. Peng, Dr. Li and Dr. Orszulik, thank you for the great memories and experiences. To Marc, Dr. Ti Chen, Dr. Jia, Dr. Peng, Dr. Ren, Dr. Li and Dr. Orszulik, thank you for taking the time to help me understand some of the concepts and for guiding me throughout my Masters. I would also like to thank my friend Anirudh with whom I took many classes with and solved many problems with.

Lastly I want to thank everyone in my family for all the support and encouragement they have provided me with. Their encouragement and support helped to reach where I am today. Finally I would like to thank Penny, who always took time out of her busy day to support me in my endeavours.

Contents

List of Tables

List of Figures

List of Abbreviations

ADRC	Active Disturbance Rejection Controller
A/D Converter	Analog to Digital Converter
DOF	Degree of Freedom
D/A converter	Digital to Analog Converter
FFT	Fast Fourier Transform
LADRC	Linear Active Disturbance Rejection Controller
LESO	Linear Extended State Observer
PEA	Piezoelectric Actuator
SDCNLab	Spacecraft Dynamics Control and Navigation Laboratory

Chapter 1

Introduction

1.1 Motivation and Objective

Piezoelectric actuators (PEAs) are examples of systems used to convert electrical energy into mechanical strain through the inverse piezoelectric effect. The inverse piezoelectric effect is when the piezoelectric material is subjected to an electric field and the dipoles are reoriented in order to store minimal electrical and mechanical energy. The resulting expansion and contraction of the crystals enable precise positioning capabilities [5]. Comparing the PEA to typical electrical motors demonstrate that PEAs do not require electrical/mechanical commutation, have the benefit of high holding torque, zero-backlash and fast response time [6]. An advantage of using PEAs is that input voltage can be controlled in order to shrink or expand the piezoelectric material very precisely. PEAs can therefore be used in applications requiring high precision movement, such as to adjust spectrometer gap spacing [7], vibration control of flexible aircraft fins [8], Atomic Force Microscopy (AFM) [9] and directional control of miniature swimming vehicles [10]. Disadvantages of using PEAs are that they experience nonlinearities such as hysteresis, creep and vibration [5]. Hysteresis is an effect in which the piezoelectric material has residual strain upon removing or reversing the applied electric field [11]. The strain is therefore dependent on the applied electric field and the history of the applied electric field. Creep is a result of the slow switching of the residual dipoles left in piezoelectric material that are not

aligned with the electric field [12]. It is observed as a slow change in PEA displacement after a sudden change in the input voltage to the PEA [13]. These nonlinearities are detrimental to PEA's positioning performance, therefore suitable controllers are required in order to achieve high-precision requirements.

There exists an extensive amount of research regarding the control of PEAs using strategies such as adaptive sliding mode controller [14], H_∞ control [15], Linear Quadratic Gaussian (LQG) [16] and PID. The motivation for this research comes from the multiple PEA system used to control the mirror gap spacing of a Fabry-Pérot spectrometer. The Fabry-Pérot spectrometer is an instrument that uses two parallel highly reflective mirrors to measure the wavelengths of light that are of interest. It has been used in the Spacecraft Dynamics and Control Laboratory (SDCNLab) in York University's stratospheric balloon flights, Fig. 1.1(a). The Fabry-Pérot spectrometer was flown twice on stratospheric balloons, first in Kiruna, Sweden, in September 2016 and most recently in April 2017 in Alice Springs, Australia, Fig. 1.1(b). It measured the albedo of the clouds and the desert, lake, trees or any ground structures. The spectrometer is used to capture images at specific wavelengths, by adjusting the spacing of spectrometer's highly reflective mirrors. The mirrors are positioned using three PEAs and must be done such that the mirrors stay parallel to each other so that an image at the desired wavelength can be captured. The wavelengths of interest were from 759 nm to 770 nm, the O2-A band which is used to determine the surface albedo [17].

The three PEA system used to adjust the mirror gap spacing is a complex system with many nonlinearities such as hysteresis, creep and thermal effects, therefore developing a dynamics model is a difficult task. The objective of this research is to use the LADRC's feature of controlling systems without detailed mathematical models to control the nonlinear three PEA system in synchronicity with only a linear estimation of the model. This investigation consists of:

(a) Achieving a steady state error within ±0.2 % of the input signal, 2 nm for a step input signal of 0.5 μm with the synchronized three PEA system. The three PEA system available for experimental purposes is a prototype of the Fabry Perot spectrometers mirror positioning system that was flown on multiple stratospheric flights. The reference input of 0.5 μm and target settling accuracy ±0.2 % are selected to be reference inputs and target error of greater settling accuracy than the Alice Springs stratospheric balloon flight where the step amplitude was 19 nm with a target accuracy of 0.1 nm [17].

(b) Analyzing the control performance when frequency of the input signal is varied. As the input signal's frequency increases, the LADRC reduces the plant to behave approximately as a double integrator. The approximate second order plant is as a low pass filter as discussed in Section 1.2. The LADRC controlled single PEA system, therefore experiences phase shifts as frequency is increased. A frequency dependent feedforward solution will be proposed and the resulting controllers tracking performance will be compared to the LADRC solution without the feedforward compensators. The controller performance evaluation criteria is to achieve an Integral Time Absolute Error (ITAE) less than 5%. This value exists as a goal for the parameter estimation algorithms to achieve. It highlights the effectiveness of the feedforward compensator and mitigates the issue of increasing phase shift as input signal frequency increases.

There exist papers in the literature addressing controllers developed to control the gap spacing of the Fabry-Pérot System [7, 16], however a solution where an accurate model of the system is not needed has yet to be studied. This directed the research focus to model independent controllers and the one that was of interest was the Linear Active Disturbance Rejection Controller (LADRC) developed by Gao [18].

The Active Disturbance Rejection Controller (ADRC) [19, 20] was initially proposed by Jingqing Han and can be summarized best in his own words as *"it inherits from proportional-integral-derivative (PID) the quality that makes it such a success: the error driven, rather than model-based, control law; it takes from modern control theory its best offering: the state observer; it embraces the power of nonlinear feedback and puts it to full use; it is a useful digital control technology developed out of an experimental platform rooted in computer simulations"* [19]. However, while ADRC is more effective for nonlinear systems, there are many parameters to determine and therefore, it is more difficult to implement. The Linear version of ADRC suggested

by Gao [18] requires only three parameters to be tuned for the systems described in this document and its performance still meets the user requirements well as will be seen later in this document.

Benefits of the LADRC include its simple design and the ability to treat hysteresis [21], vibration [22] and creep [23] as disturbances and reject them. The disturbance rejection capability along with the fact that only estimates of system parameters are required are explained in more detail later in Section 1.2. Parameters required to achieve a desired closed-loop response will be determined through a parameter estimation algorithm. Finally, experimental studies are conducted to validate the effectiveness of the proposed controller.

For simpler and more related examples, the world of athletics can be referred to. For example, there is the sport of rowing where rowers displace the water at the same time to achieve optimal velocity for the row boat. Synchronous PEAs can work together to displace large objects in coordination to each other. The aforementioned spectrometer for example, requires control over each PEA such that the differences in displacement of each actuator compared to each other is zero, establishing that the moving platform is parallel to the base.

The contribution of this research is in investigating the effect of using LADRC to control multiple PEAs in synchronicity. This research will discuss the control performance of the LADRC when a step signal is the desired tracking trajectory and for sinusoidal signals of varying frequency. The step signal is a desirable signal to track as the Fabry-Pérot spectrometer's PEAs will be provided step commands to adjust their displacement. When the desired gap spacing is achieved, the CCD in the spectrometer assembly captures the image. Sinusoidal input signals of varying frequency are compared to address implementation of the LADRC on real world systems. The LADRC exhibits low pass filter characteristics and therefore introduces a phase shift as the frequency increases. This research proposes the addition of all

pass filters to compensate for this phase discrepancy. All pass filters modify the input signal's phase across various frequencies, while applying the same gain to all frequencies. The effects of the all pass filter in the closed loop system are evaluated by comparing the fitness values of the controlled system with the all pass filter to without the all pass filter.

The outline for conducting this research is as follows, first the LADRC is introduced, next parameter estimation is addressed, then LADRC is implemented for the single PEA system, followed by the three PEA system and then the synchronous LADRC's performance is compared to an existing synchronous LQG solution.

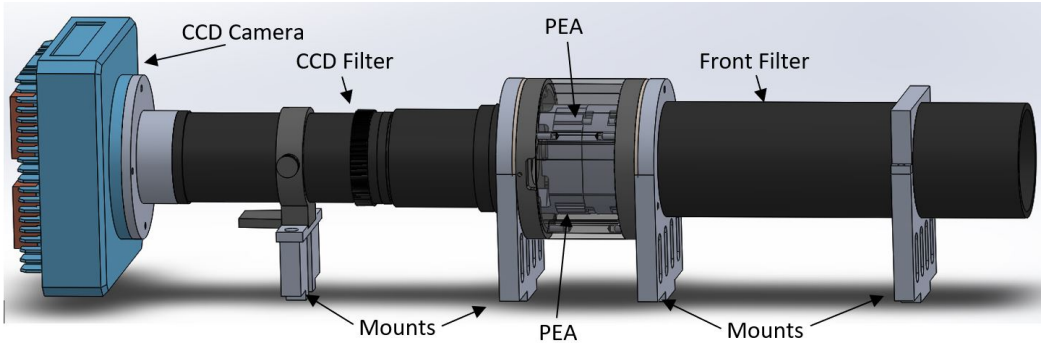

(a)

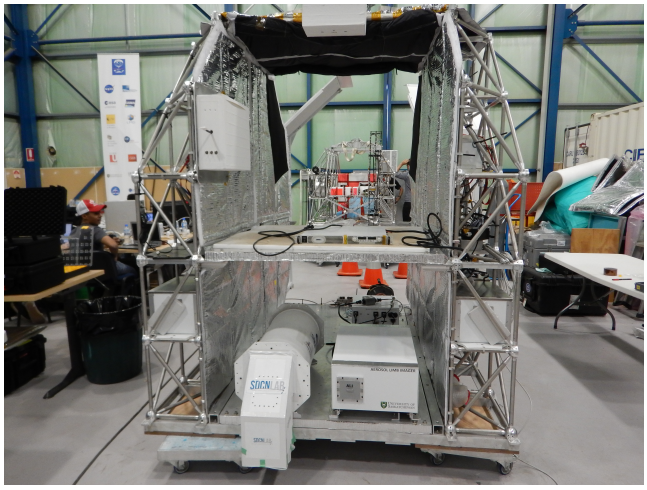

(b)

Figure 1.1: a) Fabry - Pérot spectrometer assembly; b) Fabry - Pérot spectrometer (bottom left) mounted on the balloon gondola for the stratospheric balloon flight in Alice Springs, Australia in 2017.

1.2 Introduction to the LADRC

To understand how the LADRC is designed and how it works, a brief summary from [18] will be provided.

Consider the linear second order system shown in Eq. (1.1).

$$\ddot{y} + a_1\dot{y} + a_2 y = w + bu \tag{1.1}$$

where a_1, a_2 and b are parameters defining the system dynamics and w is the external disturbance, essentially all unaccounted disturbances. Defining a generalized disturbance f in Eq. (1.2), which consists of both external disturbances and any unknown internal dynamics; Eq. (1.1) can be simplified to Eq. (1.3).

$$f = -a_1\dot{y} - a_2 y + w + (b - b_0)u \tag{1.2}$$

$$\ddot{y} = f + b_0 u \tag{1.3}$$

From Eqs. (1.2, 1.3) one will notice the addition of the term b_0. This is an estimate of the system parameter b. b_0 can be obtained from system identification or through trial and error. Any deviation from the actual system to this estimated system is therefore considered to be part of that disturbance. A poor estimate of b_0 could result in an unstable system if the ratio of $\frac{b}{b_0}$ is too large [24]. From the simplified model represented in Eq. (1.3) the observer is designed such that the generalized disturbance f is estimated as $\hat{f}$ and the plant is reduced to a double integrator as can be seen by substituting Eq. (1.4) into Eq. (1.3). This results in Eq. (1.5).

The disturbance $\hat{f}$ is estimated by the Linear Extended State Observer (LESO) as the observer state variable z_3. The observer has gains that can be selected such that z_3 is approximately equal f. This results in Eq. (1.6).

$$u = \frac{u_0 - z_3}{b_0} \tag{1.4}$$

$$\ddot{y} = (f - z_3) + u_0 \tag{1.5}$$

$$\ddot{y} \approx u_0 \tag{1.6}$$

The reduced plant is the result of the ideal LESO design and it implies that in implementation, there exists a discrepancy between the behaviour of an unit gain double integrator for the plant and its actual behaviour. Furthermore the plants nature being a second order integrator is that of a low pass filter. This means that as the input frequency increases the phase of the plant is shifted. The reduced plant, Eq. (1.6), can be controlled using a PD controller k_p (r-z_1) - k_d (z_2), defining u_0 as Eq. (1.7).

$$u_0 = k_p(r - z_1) - k_d(z_2) \tag{1.7}$$

where k_p and k_d are the proportional and derivative gains, r is the set point, and z_i represents the states of the LESO. To completely define LADRC, the LESO must be defined completely along with the closed loop system as done in Eqs. (1.8 - 1.10).

$$\dot{x} = Ax + Bu + E\dot{f} \tag{1.8}$$

$$y = Cz \tag{1.9}$$

$$\dot{z} = Az + Bu + L(y - \hat{y}) \tag{1.10}$$

x represents the states of the system, A, B, C and E are state space matrices and L is the LESO gain matrix.

$$A = \begin{bmatrix} 0 & 1 & 0 \\ 0 & 0 & 1 \\ 0 & 0 & 0 \end{bmatrix} \quad B = \begin{bmatrix} 0 \\ b_0 \\ 0 \end{bmatrix} \quad C = \begin{bmatrix} 1 & 0 & 0 \end{bmatrix}$$

$$E = \begin{bmatrix} 0 \\ 0 \\ 1 \end{bmatrix} \quad z = \begin{bmatrix} z_1 \\ z_2 \\ z_3 \end{bmatrix} \quad x = \begin{bmatrix} x_1 \\ x_2 \\ x_3 \end{bmatrix} \quad L = \begin{bmatrix} \beta_1 \\ \beta_2 \\ \beta_3 \end{bmatrix}$$

The PD controller gains are determined such that the closed-loop poles are placed at $-\omega_c$,where ω_c is the controller bandwidth. Similarly β_1, β_2, β_3 for the L matrix required to design the LESO are obtained such that the poles of the observer are placed at $-\omega_0$, where ω_0 is observer bandwidth. Placement of the ω_0 and ω_c are to ensure closed loop stability for the system.

Chapter 2

System Identification

As addressed in the introduction, one of the benefits of using LADRC is that an accurate model of the system is not required. Any deviation from the perfect definition of the system is considered to be a disturbance which could be rejected. However, a parameter b_0, which is representative of the system, needs to be known or estimated. b_0 can be obtained using system identification techniques that will be discussed in this chapter. The system identification procedure is adapted from [2, 7, 25] as it has been used to obtain the model of similar systems. System identification procedures applied for the single PEA and the three PEAs in parallel are very similar, but will be discussed separately for the sake of clarity. The process involved consists of first obtaining the response of each PEA to an input chirp signal of 0.05 V in amplitude that sweeps across the frequencies from 0 to 6000 rad/s. The reason for this range is to ensure that all the significant frequency components are addressed, as this is past the systems -3 dB cutoff frequency response and the small amplitude reduces the nonlinear characteristics of the PEA.

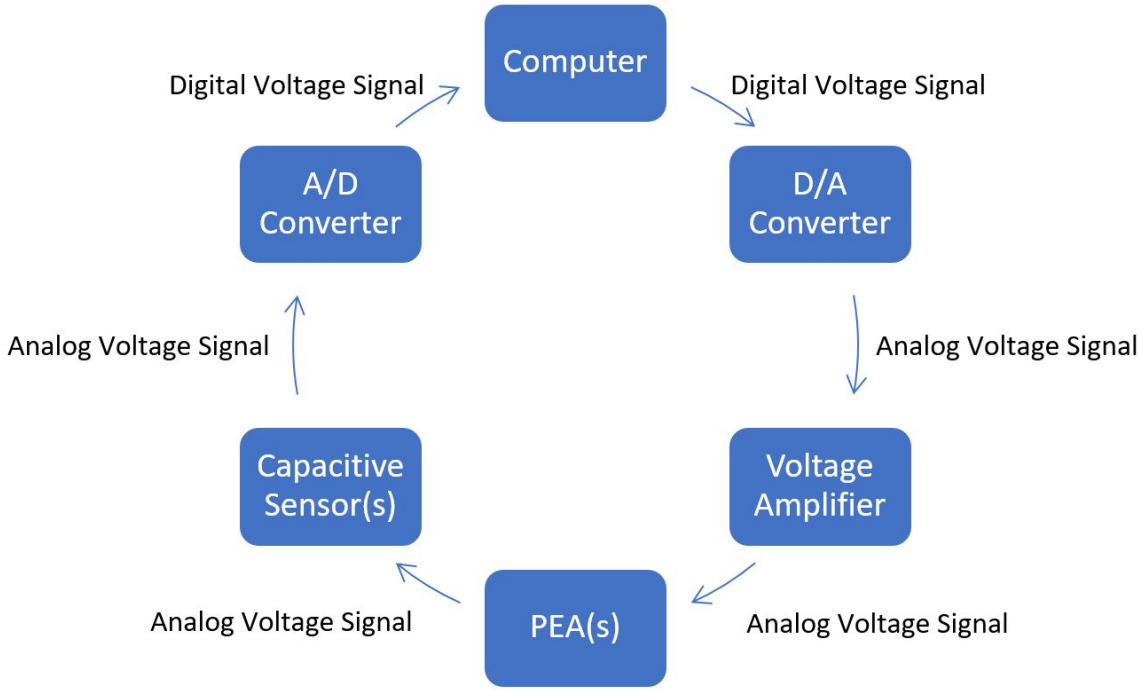

Figure 2.1: System process flow diagram

2.1 Single PEA System

2.1.1 Experimental Apparatus

The first stage of experimentation was to use LADRC to control the single PEA setup as described through Fig. 2.1. The hardware experimental process starts with a desired tracking signal generated in the computer through Matlab's Simulink toolbox. This digital voltage signal is converted to an analog voltage signal by the Digital to Analog converter (D/A converter) which is Quanser's QPIDe Data Acquisition Device. The analog voltage signal is amplified to 10x its voltage input using the E-625 voltage amplifier from Physik Instruments. The amplified voltage signal is the input of the piezoelectric stage (P-753.1CD LISA Linear Actuator and Stage from Physik Instrumente). The displacement of the PEA's moving platform from its base body, Fig. 2.2, is measured as a voltage signal using its integrated capactive sensor. The analog voltage signal is converted through the A/D converter into a digital voltage

signal and then transmitted to the computer where it will be interpreted through Simulink.

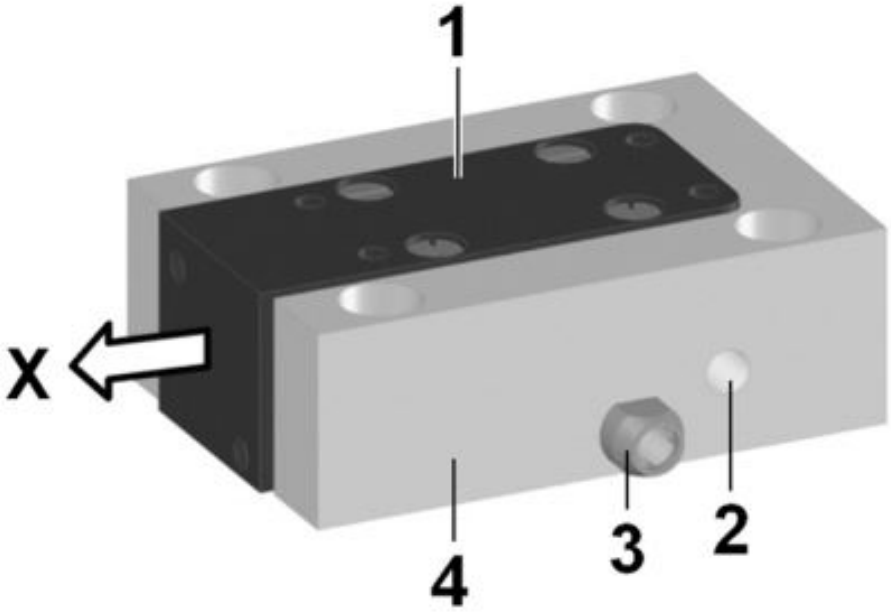

Figure 2.2: Product view from Physik Instrumente's (PI) P-753 user manual. (1). Moving Platform; (2). Protective earth connection; (3). Cable exit; (4). Base Body and X is Positive direction of motion of the stage [1].

Prior to using this setup for experimental trials, it is important to address operating constraints for the system. The input/output operating voltage range of the AD/DA converter is -10 V to 10 V, the output operating voltage range of the voltage amplifier is -30 V to 130 V and an input voltage range of -2 V to 12 V. The signal generated through Simulink is therefore restricted to the range of -2 V to 10 V.

2.1.2 Identification Procedure

The process involved consists of first obtaining the response of the PEA to an input chirp signal of 0.05 V in amplitude that sweeps across the frequencies from 0 to 6000 rad/s. Furthermore the signal being small in voltage amplitude reduces the impact of the nonlinear influences. The sweep is run for 100 s as this provides a frequency resolution of 0.01 Hz which is sufficient for this experiment. The Fast

Fourier Transforms (FFTs) of the signal input into the PEA and the output system response are taken and used to fit a transfer function best representing the system input/output characteristics. The fit of the identified transfer function can be seen through the frequency response given in Fig. 2.3 and a time domain representation is provided in Figs. 2.4 - 2.6. It should be noted that all data read from the single PEA system is subject to a measurement error. The measurement error of this system is limited by the integrated capacitive sensor resolution of 0.05 nm. It was determined that a second order transfer function, Eq. (2.1), with one zero, fits the system response to the chirp input well.

The LADRC design as introduced in Section 1.2, does not account for the zero of the transfer function. The zero is considered as part of the unknown system dynamics. The constant in the numerator of this transfer function is taken as the b_0 of system and since the frequencies of the input signals of interest for this research will be 100 Hz and below, the s term in the numerator is hypothesized to have minimal impact on the system response [26]. The results of the control experiments on the single PEA system as shown in Chapter 4 prove this approximation to be valid.

It is possible to develop an LADRC that takes the zero and other plant dynamics into account, called the Generalized Active Disturbance Rejection Controller (GADRC) [27]. However, this would mean that system identification is required to develop the controller and the controller is no longer model independent.

$$G_p = \frac{-3348s + 3.572 \times 10^7}{s^2 + 1.233 \times 10^4 s + 5.041 \times 10^7} \tag{2.1}$$

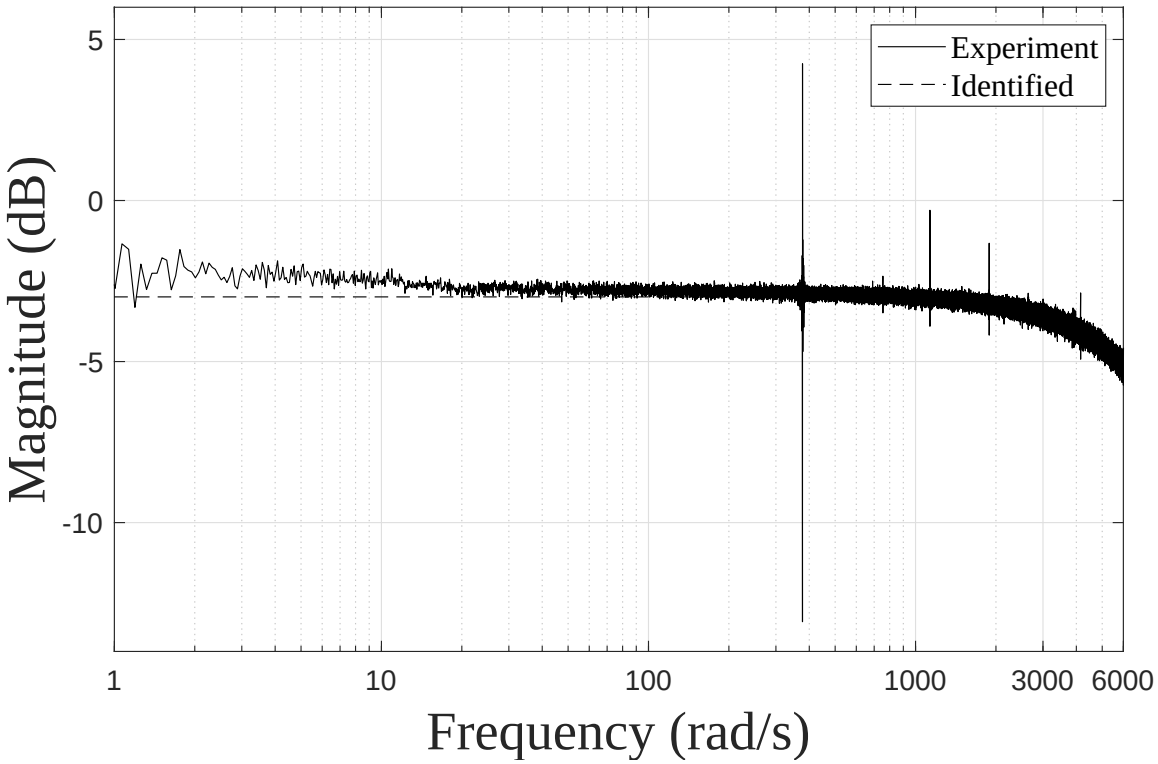

Figure 2.3: Single PEA frequency response to chirp scan from 0.1 to 6000 rad/s. The obvious frequency spikes seen in the bode plot are due to the harmonics from alternating current power line frequency of 60 Hz.

2.2 Three PEAs in Parallel Installation

2.2.1 Experimental Apparatus

The three PEA system has the same process flow diagram as the single PEA system, Fig. 2.1. The differences between the system are in the actual components used.

The three PEA system consists of three P-887.51 PEAs, an E-503.00 voltage amplifier three D-015.00 capacitive sensors with resolutions of 0.15 nm, all from Physik Instrumente. The output voltage range for the amplifier is -30 V to 130 V and the input voltage range is -2 to 12 V. Similar to of the single PEA constraint described in Section 2.1.1, this limits the input voltage to be between -2 V and 10 V at each channel (each PEA).

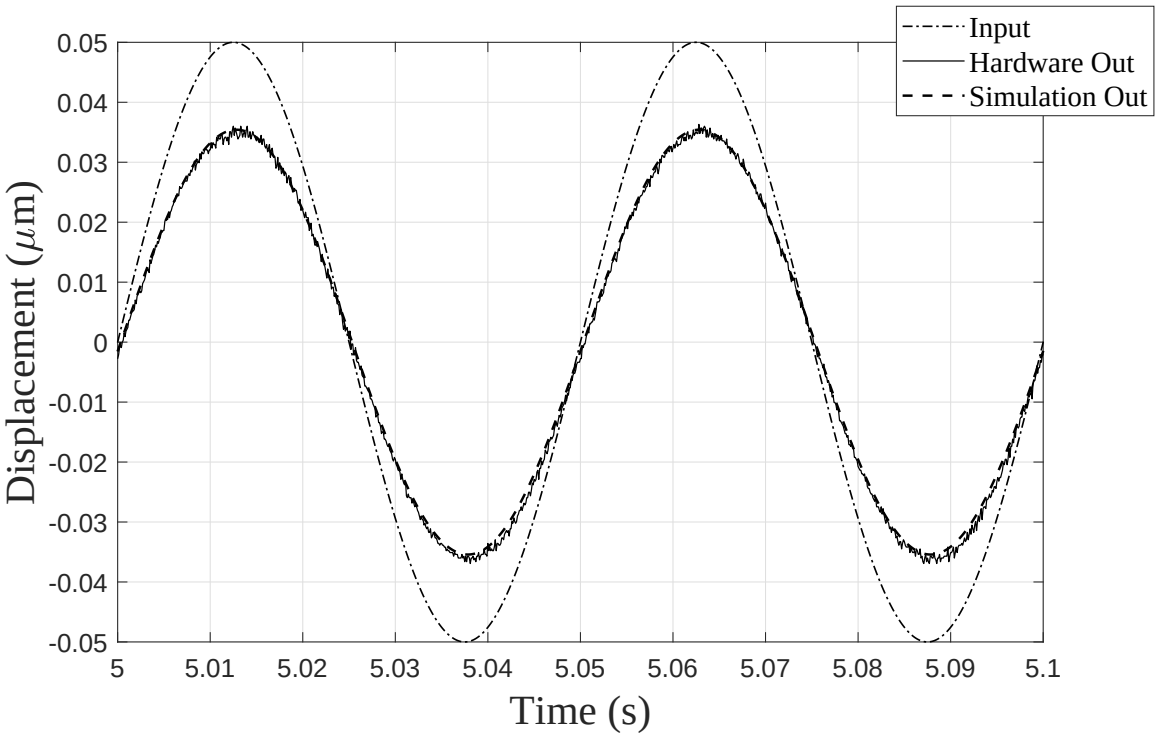

Figure 2.4: Single PEA 20 Hz open loop response

2.2.2 Identification Procedure

For the three PEAs system, Fig. 2.8, a system identification procedure similar to the one used for the single PEA system is used. In this case however, there is mechanical coupling between the three PEAs. This coupling can be observed by exciting the each PEA in the system with a step input and observing the response. When one PEA is given a step input, the other two PEAs are not provided a signal. Any resulting displacement measured by the capacitors for the other two PEAs are evidence of coupling. The resulting response is provided in Fig. 2.7. From this figure a nonzero response to the step signal is evident, thereby confirming the existence of coupling in the three PEA system.

The control goal of the three PEA system is to track one reference input signal (command) and displace each PEA in synchronicity. The desired tracking signal for all three PEAs are the same for simplicity's sake. Refer to Fig. 2.9 for an example of the system identification procedure. In this diagram only the first PEA is excited

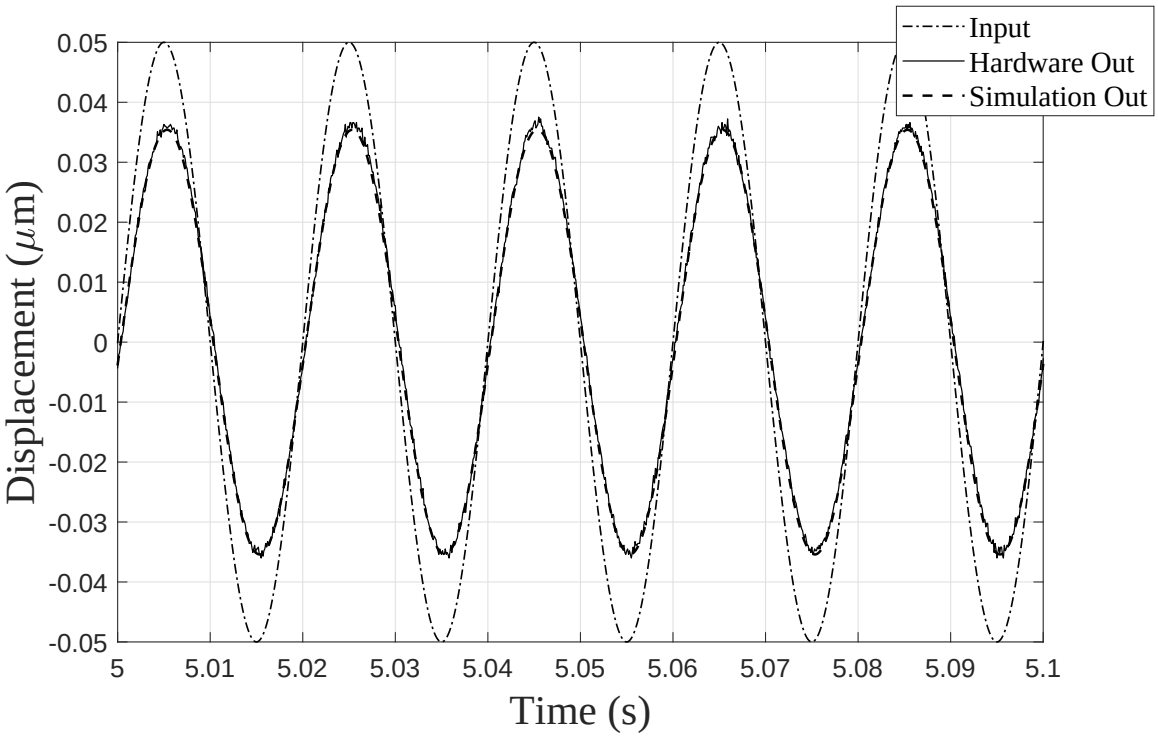

Figure 2.5: Single PEA 50 Hz open loop response

with a chirp input while the other two are fed in zero input. The voltage signals from the capacitive sensors measuring the displacement of the moving platforms of the PEAs are then converted to their micrometer interpretation. The *remove bias* blocks essentially ensures that the positions of the PEAs are taken to be zero at initialization, when time is zero and any proceeding displacements are offset from this position.This is accomplished by removing any initial capacitive sensor voltage offsets. The PEAs and the capacitive sensors are not collocated [28], so a geometric correction block is placed at the end to correct for the lack of collocation.

System identification of the three PEA system is accomplished by obtaining a frequency response of each PEA while the other two PEAs are not given any input. The frequency responses are then used to obtain nine transfer functions for the system. The chirp signal is input into one of the PEAs and the output being the displacement of the PEA stage measured at each one of the capacitive sensors. The determination of each transfer function is done in the same manner as it was done for the single

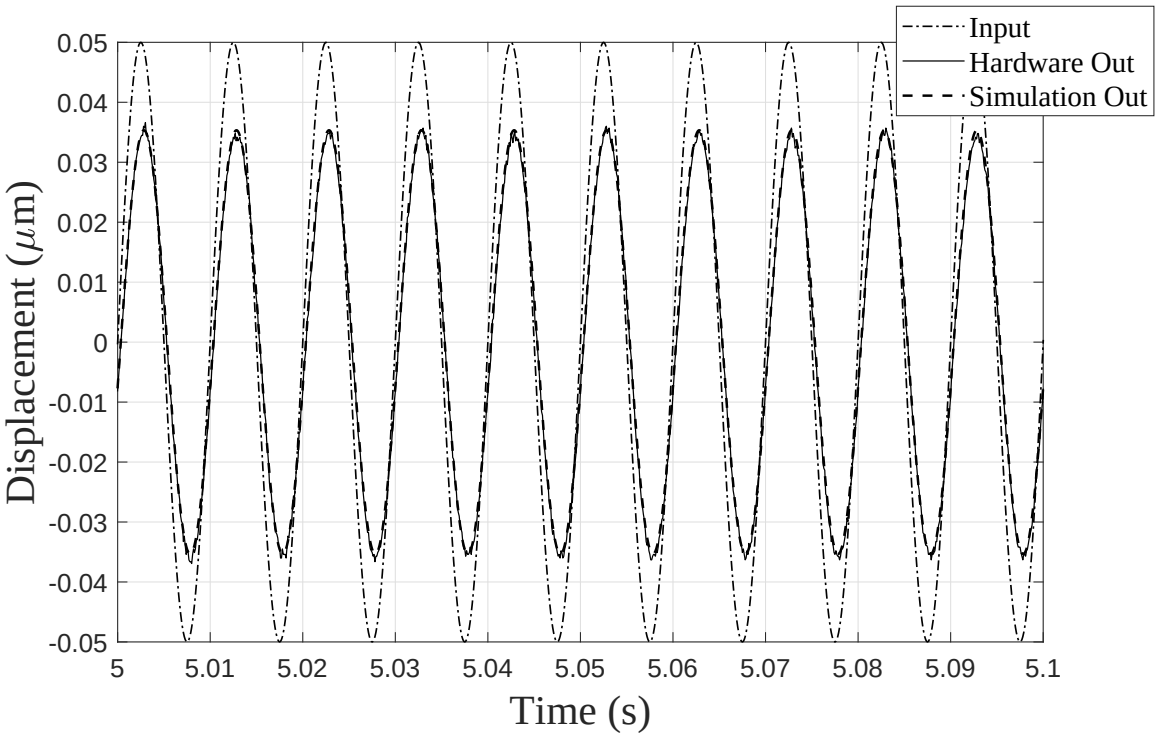

Figure 2.6: Single PEA 100 Hz open loop response

PEA. The FFTs of the channels' input and output response are taken and used to fit a transfer function best representing the system's input/output characteristics [12]. This procedure resulted in nine second order transfer functions (refer to Table 2.1), that fit the input/output characteristics of the system best. To demonstrate how well the transfer function matches the real system, the system is excited with 20 Hz, 50 Hz and 100 Hz sinusoidal signals. The resulting time domain responses of the real system and the simulink response are compared Figs. 2.10-2.12. The fit of the identified transfer function is also provided in through the frequency response given in Fig. 2.13. It should be noted that all data read from the three PEA system is limited by the capacitive sensor's resolution of 0.15 nm.

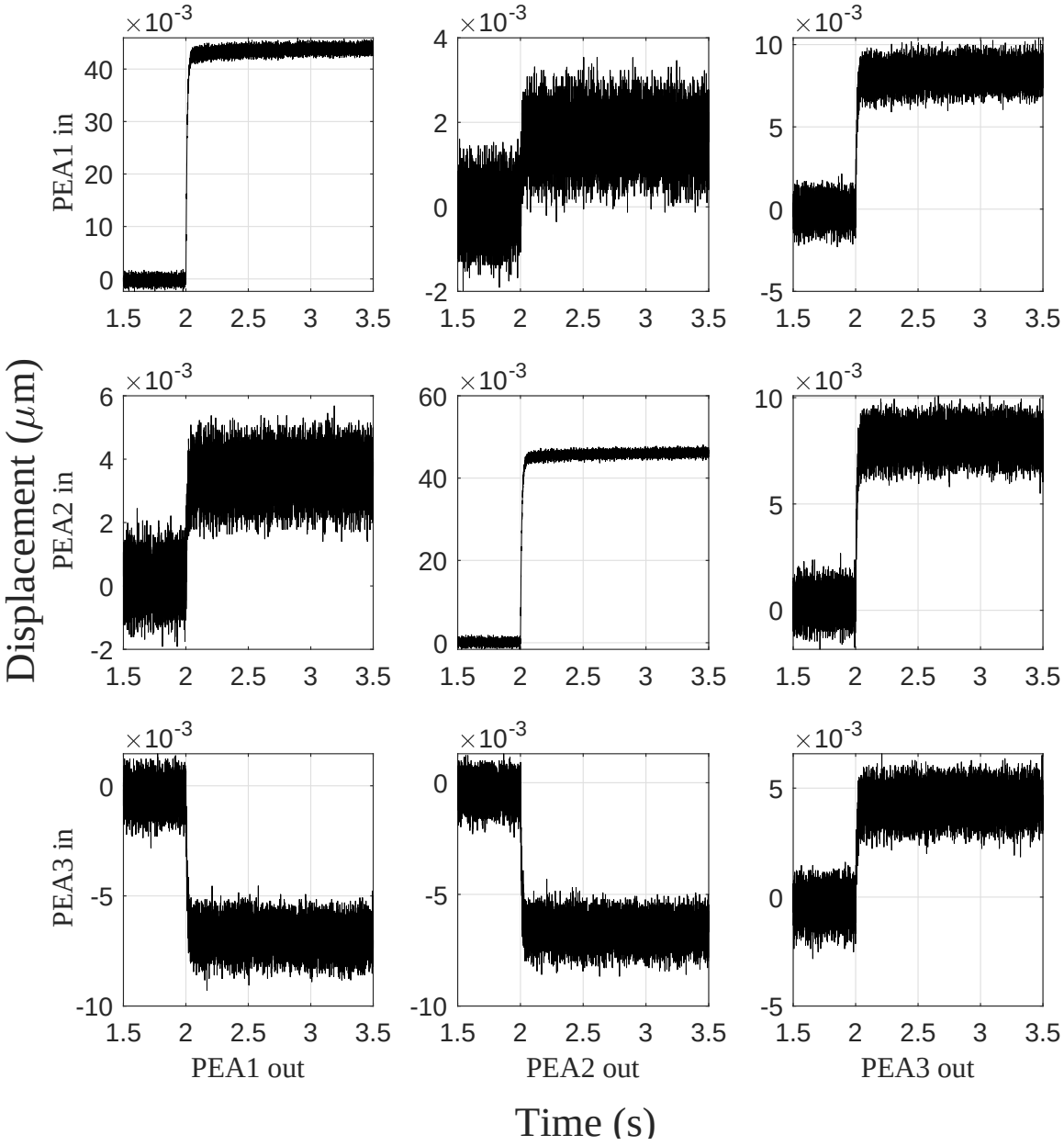

Figure 2.7: Response of the three PEAs to a 0.05 V step signal. The off-diagonal graphs show coupling between the PEAs.

Table 2.1: Three PEA 3 × 3 transfer function matrix

Output / Input	**PEA 1**	**PEA 2**	**PEA3**
PEA 1	$\frac{-49.867s+2.4120\times10^5}{s^2+2.7575\times10^3s+2.8308\times10^5}$	$\frac{-2.1580s+1.1435\times10^4}{s^2+3.1875\times10^3s+2.7910\times10^5}$	$\frac{-9.5810s+4.5952\times10^4}{s^2+2.7826\times10^3s+2.8261\times10^5}$
PEA 2	$\frac{-3.1762s+1.6303\times10^4}{s^2+2.8060\times10^3s+2.4298\times10^5}$	$\frac{-48.638s+2.2871\times10^5}{s^2+2.7229\times10^3s+2.5935\times10^5}$	$\frac{-9.5810s+4.5952\times10^4}{s^2+2.7826\times10^3s+2.8261\times10^5}$
PEA 3	$\frac{7.8555s-3.5297\times10^4}{s^2+2.8198\times10^3s+2.9274\times10^5}$	$\frac{7.3918s-3.2991\times10^4}{s^2+2.7947\times10^3s+2.8996\times10^5}$	$\frac{-9.5810s+4.5952\times10^4}{s^2+2.7826\times10^3s+2.8261\times10^5}$

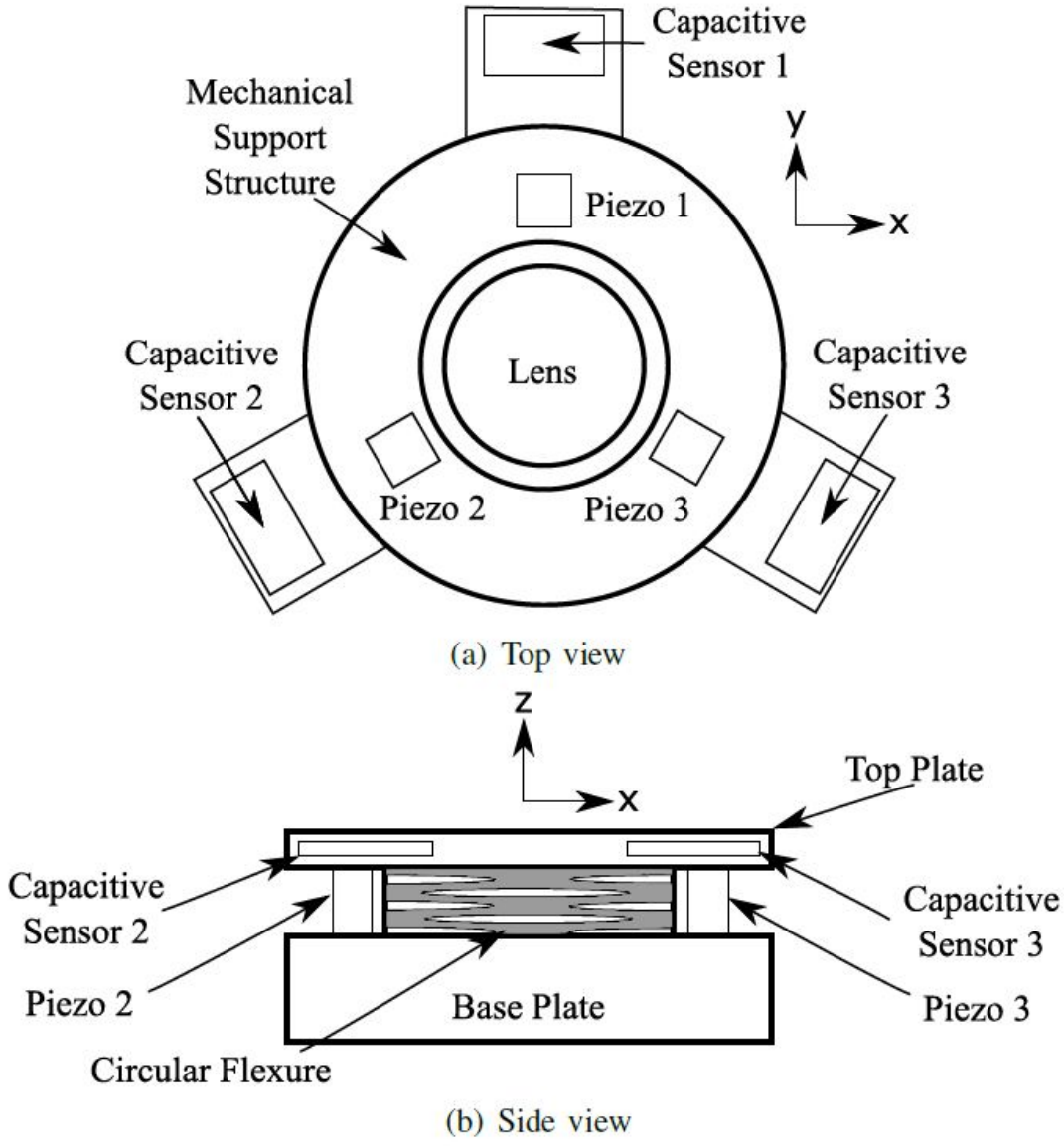

Figure 2.8: Three PEA system schematic diagram. From figure a) it can be seen that the sensors and actuators are not collocated, therefore requiring a geometrical correction when analyzing the output.Furthermore, it should be noted that the direction of displacement of the PEAs are in the Z axis [2].

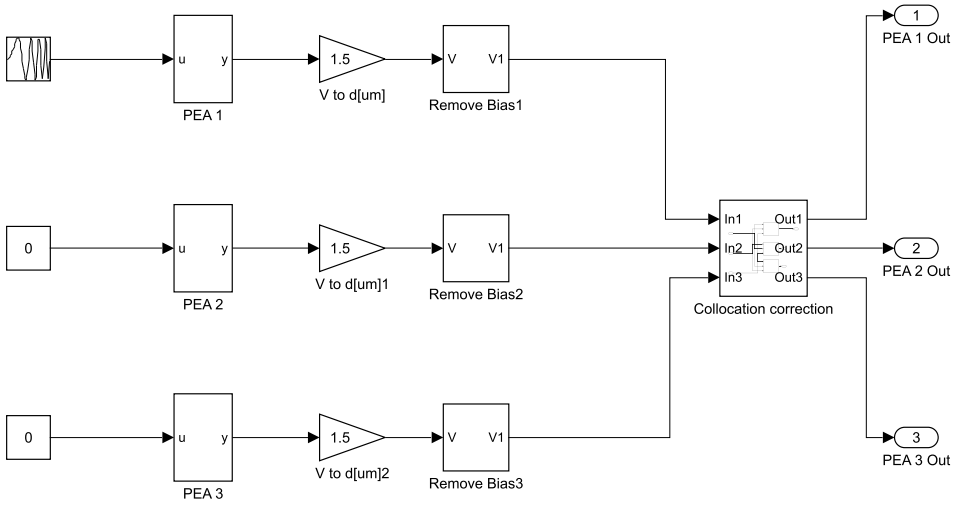

Figure 2.9: Three PEA system identification block diagram used in Matlab Simulink.

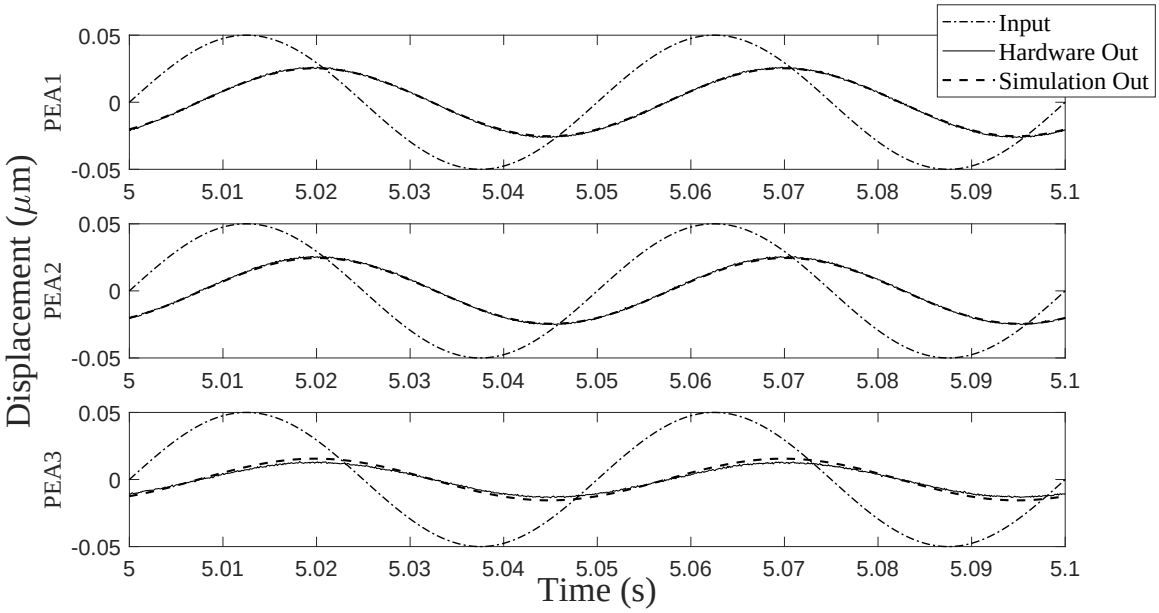

Figure 2.10: Three PEA 20 Hz open loop response

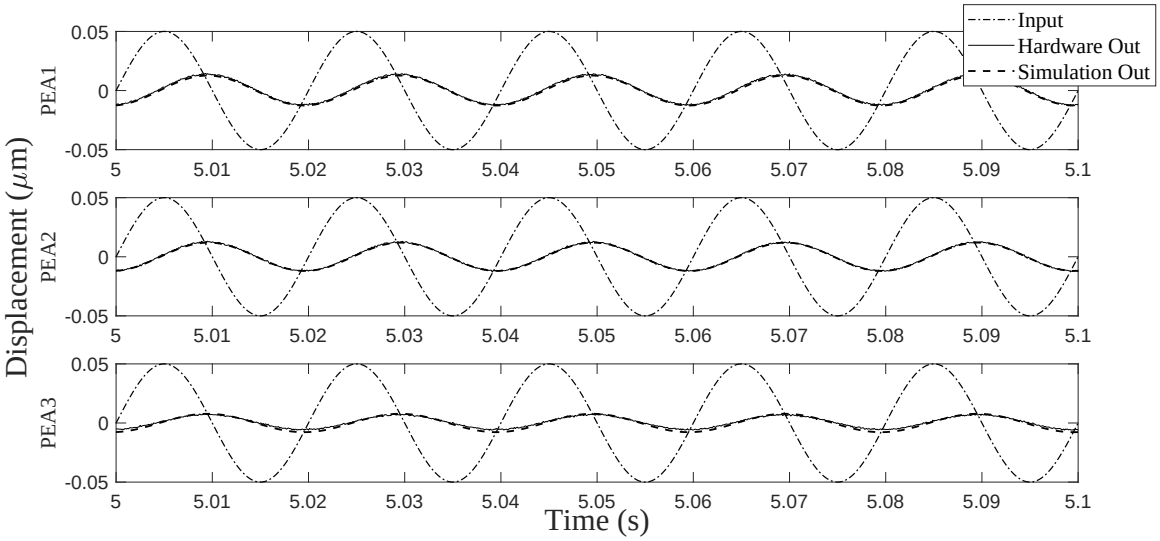

Figure 2.11: Three PEA 50 Hz open loop response

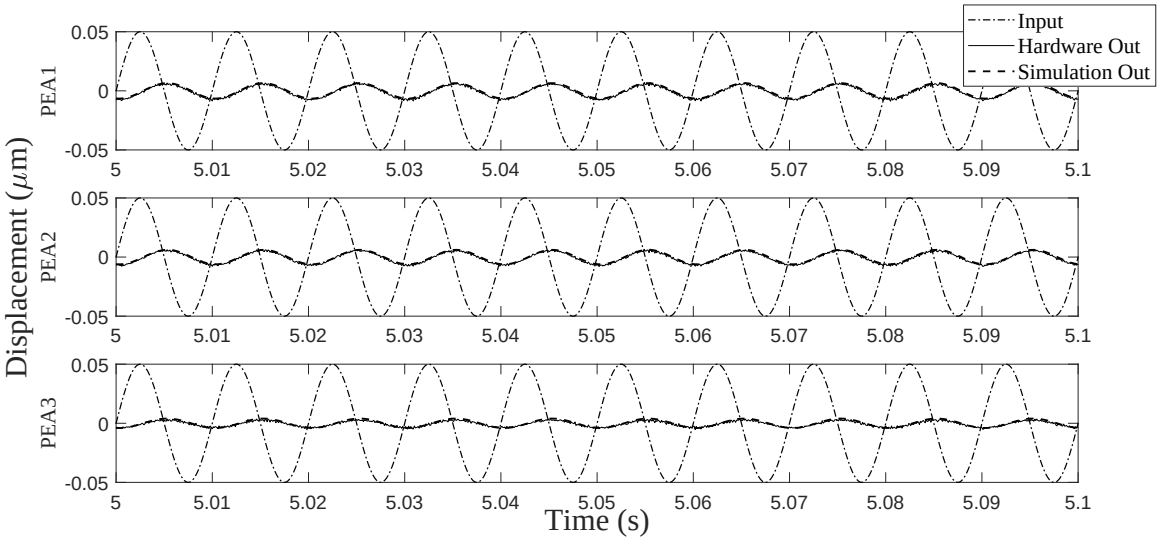

Figure 2.12: Three PEA 100 Hz open loop response

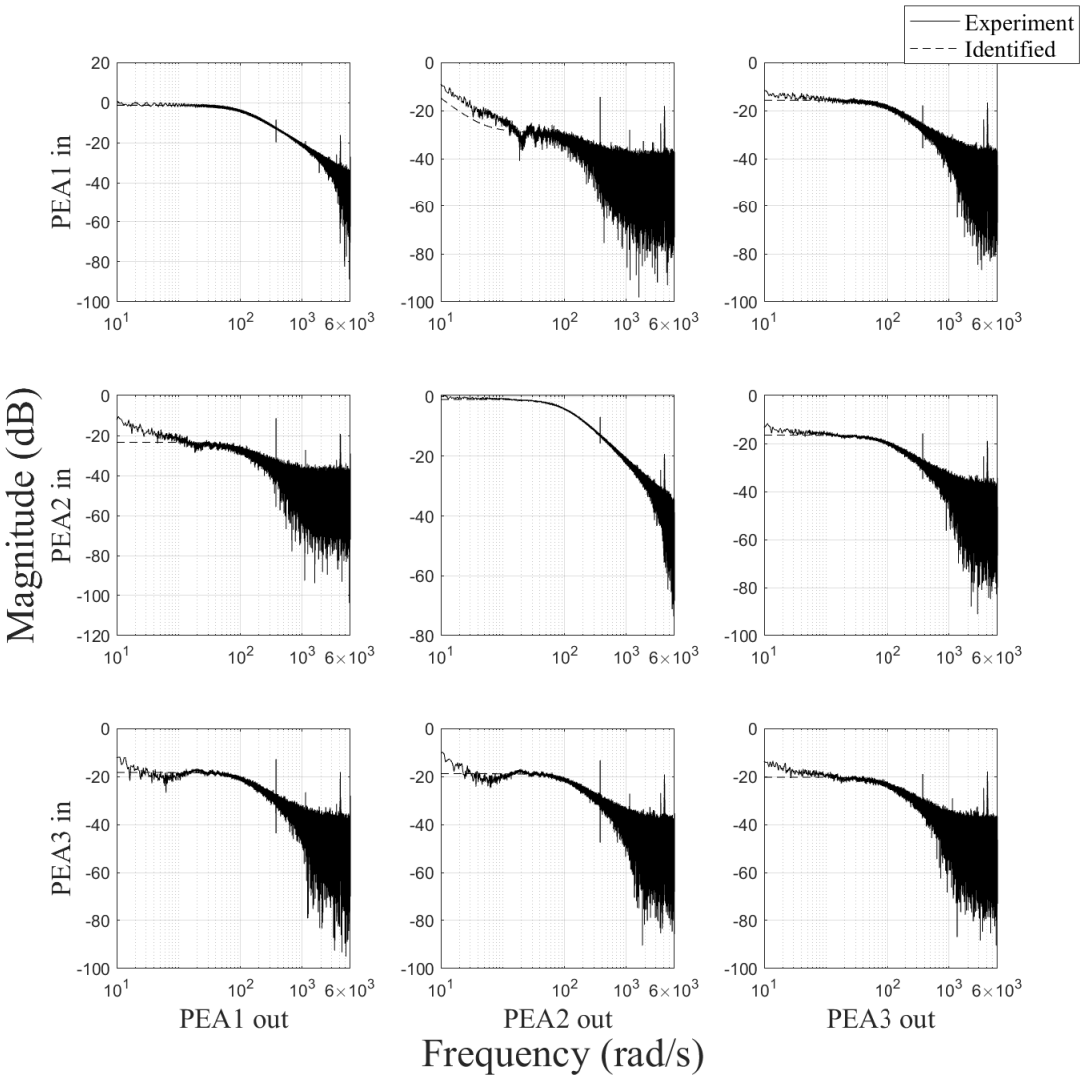

Figure 2.13: Three PEA frequency response to chirp scan from 0.1 to 6000 rad/s. The obvious frequency spikes seen in the magnitude plots in positions (1,1), (2,2) and (3,3) are due to the harmonics from alternating current power line frequency of 60 Hz.

Chapter 3

Parameter Estimation

The LADRC design introduced in Section 1.2 is for a single PEA. The construction of the controller scheme for multiple PEAs is similar and will be discussed in more detail in Chapter 5. Now that the parameters of interest have been identified, it is necessary to discuss of ways to obtain them.

Three methods of parameter estimation will be discussed; Taguchi's method, Genetic algorithm and the Brute-force method (exhaustive search method). These methods can be used for controllers other than ADRC or LADRC as well. It is up to the discretion of the control engineer to determine which method should be used for their application. There are other applicable methods, however Taguchi's method is rather novel in the field of control systems, whereas the Genetic-algorithm is well known and commonly used. The Brute-force method too is well known, however it is not the best solution when searching in large solution spaces where high parameter precision is required, as will be demonstrated in Section 3.6. The Brute-force method will provide perspective on how efficient the Genetic algorithm and Taguchi's method are in comparison.

3.1 Fitness Function

The objective function to minimize in this case would be:

$$\sum_{i=1}^{n} |y(i) - r(i)|\delta t \tag{3.1}$$

where i is the sample number, n is the total number of samples, $y(i)$ is output at the i-th sample, $r(i)$ is the sampled i-th input and δt is time interval per time step.

Eq. (3.1) is referred to as the Integral Time Weighted Absolute Error (ITAE). ITAE is the selected system performance measure because it focuses on achieving a lower settling time and faster convergence [29]. A lower settling time would mean that the desired motion would be tracked faster. Faster tracking for each PEA results in a faster synchronization of the system which is desired so that more images can be captured with the Fabry-Pérot spectrometer within a specific time frame. The ITAE is then divided by a summation of the truth values (the desired trajectory to track) over time to get the relative error which is then multiplied by 100% to get the relative percentage error as shown in Eq. (3.2).

$$FitnessValue = \frac{\sum_{i=1}^{n} |y(i) - r(i)|}{\sum_{i=1}^{n} |r(i)|} 100\% \tag{3.2}$$

It is important to note that running the optimization algorithm with this fitness function may provide acceptable results for some particular cases, but these results can be significantly improved by placing constraints on the solution from which the parameters are selected. This concept will be elaborated in Section 3.5.

3.2 Taguchi's Method

Taguchi's method is a global optimization method. It uses orthogonal arrays to reduce the number of experiments required to satisfy the end condition. A matrix A of N rows and k columns composed of elements from a set of levels, S, is called an orthogonal array with strength t ($0 <= t <= k$) and s levels if in every N by t sub

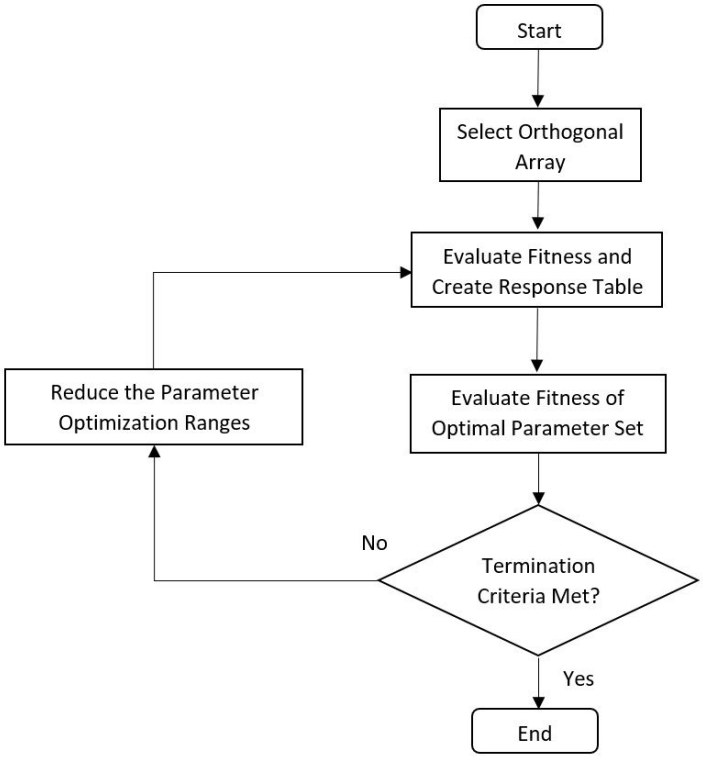

Figure 3.1: Taguchi's method flowchart [3]

array of A, each t strength tuple combination of S appears exactly the same number of times as a row [30].

It is necessary to discuss the design of the orthogonal array when discussing the Taguchi's method. Orthogonal array selection is dependent on the number of parameters in the experiment and the complexity of the optimization problem. For example, consider an orthogonal array of 10 columns, $k = 10$; three levels, $S = 1, 2, 3$; strength $t = 2$; and 27 rows, $N = 27$. Pick any 2 random columns and one would get any one of the 9 possible combinations of (1,1), (1,2), (1,3), (2,1), (2,2), (2,3), (3,1), (3,2) and (3,3). The number of columns represent the number of parameters for the experiment and the row number represents the number of experiments (calls to the fitness function). This orthogonal array is selected to have a strength of 2, meaning that only combinations of two parameters are considered. Larger values can be selected at the expense of more calls to the fitness function. This orthogonal array

also has three levels, meaning the optimization ranges for each parameter is divided into three levels. The levels are maps to other numerical values, each parameter may have a different mapping for the levels and furthermore the levels are bounded by the limits of the parameter. The number of levels can be increased as well at the expense of more calls to the fitness functions.

For this research a strength of two and three levels are used for all parameter estimation problems as the target fitness values were achieved. Constructing the orthogonal array will not be discussed in detail, since for this research orthogonal arrays are obtained from the online database in [31]. When selecting the orthogonal array, the user needs to keep in mind of the number of experiments, number of parameters for the experiment and also the number of levels and the strength.

Taguchi's method can be implemented by dividing the process into the following steps and referring to the flowchart shown in Fig. 3.1:

(a) Design the fitness function as discussed in Section 3.1.

(b) Select an appropriate orthogonal array and identify the mapping for the levels corresponding to each parameter.

(c) Run the experiments and build the response table.

   i The response table identifies best fitting level for a parameter. The best fitting level for each parameter is obtained and used to get the best fitting parameter for that generation of the algorithm

   ii This combination of best fitting parameters is run to obtain its fitness value and is the optimal fitness for that generation

(d) Check if the result obtained meets the termination criteria, if so end.

(e) If the termination criteria is not met reduce the optimization range, go to step (b) redefine the level mappings corresponding to each parameter in the orthogonal array and continue to iterate through the list again until the termination criteria is met.

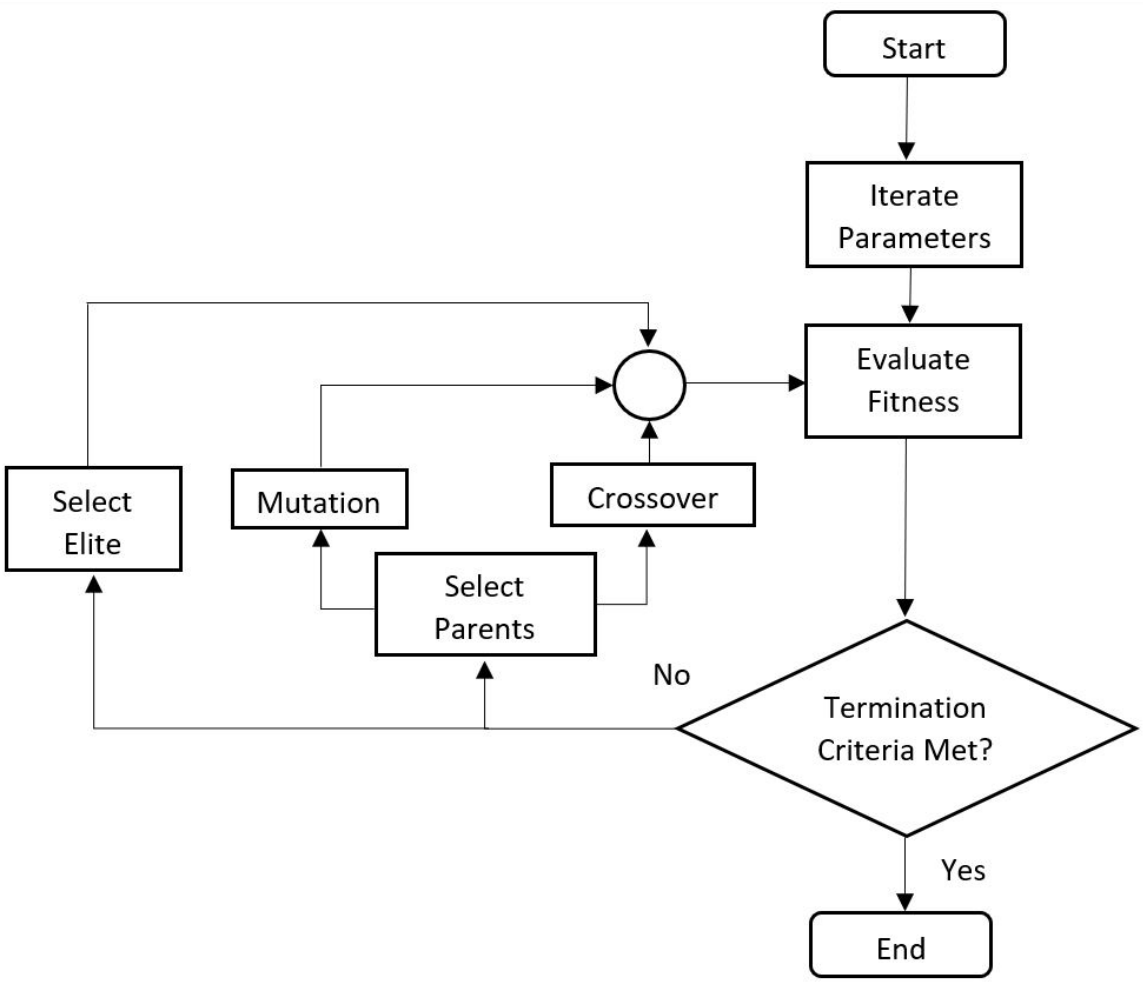

Figure 3.2: Genetic algorithm flowchart

3.3 Genetic Algorithm

Genetic Algorithms were introduced by John Holland in the 1960s. It uses the evolutionary process from biology to solve global optimization problems. The general concept is that of a survival of fittest and is described in the flowchart show in Fig. 3.2. From an initial population, the strongest members will survive and mate to create the next generation. The next generation would have traits from their parents and again only the strongest would reproduce. The algorithm works similarly, such that the fitness values from an initial population of stochastically determined objects containing parameter sets is obtained.The sets resulting in fitness values closest to the desired fitness are considered elite and taken to be in the next generation. Each generation proceeding the initial inherits parameters that were common with the parents and have parameters that weren't common with the parents. There will also be some mutation of parameters, random parameter selection that are independent from the parent parameter set. This allows for a greater traversal of the solution space and enables the algorithm to find a global solution. For this research Matlab's built in ga() function is used [32, 33].

3.4 Brute-Force Method

The Brute-force method consists of a combination of trial and error approaches and control techniques to verify stability. As mentioned before a trial and error approach to determine parameters may be implemented. Unfortunately, in the worst case the user a full factorial experiment which can be very time consuming and memory exhaustive will need to be conducted.

The algorithm's flowchart is provided in Fig. 3.3. A description of the process is provided as follows:

(a) Select upper bounds, lower bounds and a discrete step size for each parameter.

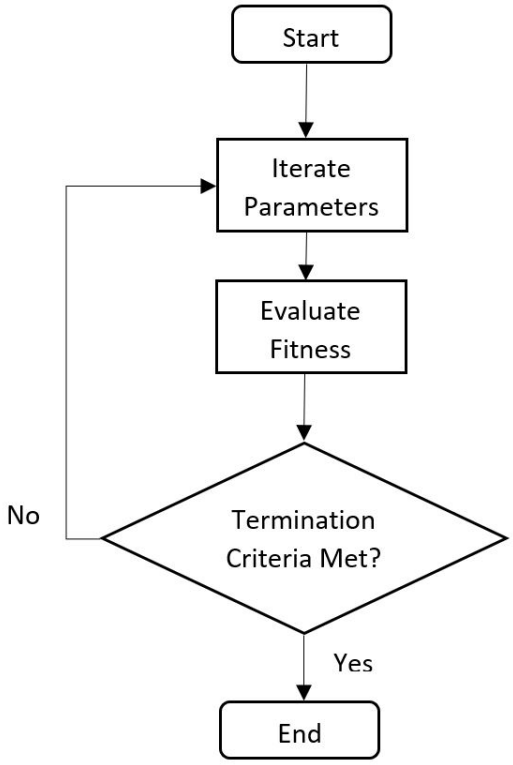

Figure 3.3: Brute-force method flowchart

For example if the upper bound and the lower bound for a parameter, B, is 1000 and 0, given a step size of 1, there exist 1001 possible discrete values for parameter B.

(b) Obtain a parameter set as a combination from the list of all possible parameter combinations for the specified bounds and discrete step size.

(c) If the fitness requirement is met then the parameters are appropriate, if not go back to step (b) and and iterate to next combination of parameters in list. The list of possible parameter combinations would be traversed and the fitness is calculated until the desired fitness value is achieved or another termination criterion, such as the computer running out of allocated memory, is triggered.

3.5 Parameter Bounds

Regardless of which parameter estimation algorithm is selected, narrowing the parameter bounds will reduce the computation time required to determine a set of parameters that satisfy the fitness value requirement. For example as mentioned in

Sections 2.1.1 and 2.2.1, the hardware used to validate the control strategies possess operating voltage constraints. The amplifier has an operating range from -2 V to 12 V and the DAC has an operating range from -10 V to 10 V. The system input will be therefore limited to a range of -2 V and 10 V. The LADRC faces the same limitation for the input to the plant. However the LADRC has the additional limitation for the parameter, ω_0 [24]. While larger values of ω_0 are preferred for the LADRC, as this is required to justify approximating the plant as a double integrator, the issue that arises is that at large ω_0, the system is more susceptible to noise [34]. As discussed in [24], increasing the b_0 parameter may permit larger ω_0, however this would be an additional parameter to estimate or three in the case of the synchronized LADRC. Another possible solution is to search for the same parameters, but factor in the noise as part of the simulation. The resulting set of parameters would be able to achieve the desired fitness in the presence of the expected noise.

Other than the operating limitations of the hardware, there are other constraints that can be placed on the parameters to narrow the solution space. For example, if the user has a constraint on their solution space that bounds the permitted overshoot, taking the best solution as the result of minimizing the relative percent ITAE would be an issue. The ITAE would only sum up the absolute value of the error multiplied by time over a time frame and the optimization algorithm would minimize for this, meaning that in the event that overshoot is large but has small overall area in comparison to low overshoot but larger area, then the higher overshoot response would be seen as a preferred solution. Since this result does not satisfy the user's requirements, they may add a penalty to the output of the ITAE. In the event overshoot is above a certain threshold or exists for too great a time duration, the resulting ITAE calculation can be summed with overshoot multiplied by a weight factor or infinity depending on importance of having the constrained overshoot [35].

3.6 Comparison of Parameter Estimation Methods

Having discussed three different parameter estimation methods, a suitable method must be selected for this research. A method of achieving this is to use all three methods on the plant, obtain the parameters and compare the system performance. However, this method does not indicate that any of the three solutions actually provide global convergence, hence the accuracy of convergence for each optimization method must be considered as well. Therefore, the optimization methods will be used to find the optimal parameters for a mathematical function with a known analytical optimal parameter set. The function will have multiple peaks and troughs to ensure that the algorithm finds global optimal solution.

The research consists of controlling both a single PEA and three PEAs in synchronicity. In the case of the single PEA a minimum of two parameters require tuning for the LADRC, if the b_0 parameter is estimated using a system identification approach as opposed to a parameter estimation algorithm. To control three PEAs in synchronicity the LADRC requires seven parameters to be tuned, as will be explained in Chapter 5. For any number of parameters, there may not be a single optimization algorithm that can be considered faster and more accurate than all the others. To determine whether this is the case, the Genetic algorithm, Taguchi's method and the Brute-force search method will be used to find the global minima over a fixed domain.

The first case studied will compare the performance of the three optimization algorithms in the case of a single parameter. Determining the global minima of Eq. (3.3) will be used as the first measure to compare the performance of the three algorithms.

$$\begin{aligned} y(a) =& (a+2)(a-4)(a+3)(a-5)(a-7)(a-8)(a-1)(a-9), \\ & -10 \leq a \leq 10 \end{aligned} \tag{3.3}$$

This function has local minima between the domain of -10 and 10 and a global minima of -5.1158e+04, which was calculated analytically. Using the analytically calculated global minimum, y_{min}, as the true minimum, a fitness function for the optimization algorithm is developed to minimize the difference between the y_{min} and $\hat{y}_{min}$ (y_{min} calculated from parameter estimates).

The performance of the algorithms must also be compared in cases where greater numbers of parameters are required to be optimized. From this, one can extrapolate any evident patterns in how the algorithms behave as the number of parameters increase. To do this, the number of iterations required to obtain a solution that is within 1% of the true value (determined analytically) is compared between the three algorithms. The results are displayed in Table. 3.1 and the functions for which the algorithm was searching for are shown in Eqs. (3.3-3.6).

The low number of calls to the fitness function is important when determining an acceptable parameter set for the controller because the fitness value is determined from the results of a Simulink simulation where a long computational time is possible, depending on the complexity of the simulation. The test to determine the global minima for the single parameter equation indicate that the Taguchi's method is the best choice of the three considered algorithms when a tight fitness requirement exists.

The same tests are repeated for the cases of the two parameter function in Eq. (3.4), four parameter function in Eq. (3.5) and seven parameter function in Eq. (3.6).

$$\begin{aligned} y(a) =& (a+2)(2a-1)(a-3)(2.5a+4)+ \\ & (b+2.5)(2b-1.5)(3b-3.5)(b+4.5), \end{aligned} \tag{3.4}$$

$$-50 \leq a \leq 50, -50 \leq b \leq 50$$

Table 3.1: Comparison of the number of calls made to the fitness function by different optimization algorithms for different numbers of parameters

Number of Parameters / Optimization Algorithm	1	2	4	7
Genetic algorithm	250	650	500	3400
Taguchi's method	162	360	306	702
Brute-force method	7000	520984	19375483	$\leq 1.3255 \times 10^{16}$

$$
\begin{aligned}
y(a,b,c,d) =& (a-1)(a+2)(a+3.2)(a-0.5)+ \\
& (2b-0.2)(3b+1.5)(2.1b+8)(0.2b-0.3)+ \\
& (1.2c-0.4)(2c+0.3)(0.1c+10)(0.5c-3)+ \\
& (3d-0.9)(2.2d+1.6)(0.6d+0.3)(0.9d-2.8), \qquad (3.5) \\
& -100 \leq a \leq 100, -100 \leq b \leq 100, \\
& -100 \leq c \leq 100, -100 \leq d \leq 100
\end{aligned}
$$

$$
\begin{aligned}
y(a,b,c,d,e,f,g) =& (a-1)(a+2)(a+3.2)(a-0.5)+ \\
& (2b-0.2)(3b+1.5)(2.1b+8)(0.2b-0.3)+ \\
& (1.2c-0.4)(2c+0.3)(0.1c+10)(0.5c-3)+ \\
& (3d-0.9)(2.2d+1.6)(0.6d+0.3)(0.9d-2.8)+ \\
& (2.1e-4.2)(3.6e+0.5)(0.7e+2)(1.3e-2)+ \\
& (2.8f-1.3)(4.2f+5)(0.2f+8)(2.3f-0.7)+ \\
& (4.3g-3.8)(2.9g+4.8)(2.3g+0.1)(1.7g-2.7) \qquad (3.6) \\
& -100 \leq a \leq 100, -100 \leq b \leq 100, \\
& -100 \leq c \leq 100, -100 \leq d \leq 100, \\
& -100 \leq e \leq 100, -100 \leq f \leq 100, \\
& -100 \leq g \leq 100
\end{aligned}
$$

From Table. 3.1 it is observed that as the number of parameters increase the number of calls to the fitness function increase as well. The Brute-force method stands out in how many calls it made to the fitness function in order to achieve a solution that met the fitness requirement. Furthermore it should be noted that the Brute-force method was not used to achieve a solution for the seven parameter case,

because the number of calls to the fitness function are too great for the algorithm to make in a reasonable amount of time. Instead, a worst case solution is provided, which specifies that a total of 1.3255×10^{16} calls to the fitness function are be made if the traversal is started from the furthest point away from the solution. This leaves just the Genetic algorithm and Taguchi's method out of the three candidates to be parameter estimation algorithm used in this research.

Selecting between Taguchi's method and Genetic algorithm for the parameter estimation algorithm proves to be more challenging than deciding to eliminate the Brute-force method from the candidacy. Both algorithms have many modifiable characteristics, for example in the case of the Taguchi there is a modifiable convergence rate rr for each parameter under investigation. This parameter reduces the range within which the parameter is searched for. The parameter has a value between 0.5 and 1, but the greater in value it is, the slower the algorithm converges [30]. This is because the range will not change as fast and hence the solution space will not be explored as quickly. Increasing rr will decrease the convergence rate but more experiments will be conducted within the parameter bounds; this is required if the desired fitness requirement is not achieved. This is a trade-off been convergence speed and accuracy that exists within the Taguchi's method. The Genetic algorithm has a mutation aspect where a parent parameter set's component is modified at random and when the children parameter vectors are created they would carry this trait. The more probable the event of mutation, the greater the traversal that could occur. If mutation parameter is too great, then convergence is not guaranteed. These are just examples of ways that the algorithms can be modified. Given the stochastic nature of parameter selection of genetic algorithms, it is not possible to guarantee a precise number of generations under which a parameter set resulting in a fitness that satisfies user requirements is obtained. However if the stochastic nature is selected to be Gaussian, as Matlab's genetic algorithm is by default, then an average value of the

number of generations required for the convergence to be achieved can be calculated. Simply comparing the number of calls made to the fitness function for the seven parameter case, the Genetic algorithm required a greater number of calls than Taguchi's method. Similarly in the case of the four, two and single parameter optimization, the Genetic algorithm required more calls than Taguchi's method. Taguchi's method has demonstrated greater reliability than the Genetic algorithm in requiring a fewer number of calls. Therefore Taguchi's method will be used to determine the parameters for the single PEA and the three PEAs.

Chapter 4

Single PEA Control Using LADRC

Given that the system plant is identified and a parameter estimation algorithm is selected, the next step is to control the plant. While system identification isn't necessary for LADRC, it reduces the error that needs to be corrected by the controller compared to when guessing the system parameter b_0 is guessed. Hence, from system identification in Chapter 2, it is understood that both the single PEA and the three PEAs in parallel installation are represented using second order transfer functions.

Recall the LADRC design discussed in Section 1.2.

$$\ddot{y} = (f - \hat{f} + u_0) \tag{4.1}$$

where $\hat{f}$ will be estimated using the Linear Extended State Observer (LESO). LADRC will be composed of a PD controller and the LESO. The LESO's observer gain vector, L, can be designed such that the error between the estimated disturbance and actual disturbance will be very small. This simplifies the plant to a simple unit gain double integrator, Eq. (4.3).

$$\ddot{y} = u_0 \tag{4.2}$$

$$u_0 = k_p(r - z_1) - k_d(z_2) \tag{4.3}$$

Where r is reference signal, z_1 and z_2 are the first and second estimated states from

the LESO.

This will be controlled by the PD controller. The L vector is constrained such that the eigenvalues of the observer lie in the left-half plane and similarly the controller eigenvalues are in the left-half plane. These are the required conditions that must be met for observer and controller stability and therefore closed loop stability.

Observer Stability:

$$Re(eig(A + LC)) < 0 \tag{4.4}$$

Controller Stability:

$$Re(eig(A + BF)) < 0 \tag{4.5}$$

where

$$F = -\frac{1}{b_0}\begin{bmatrix} kp & kd & 1 \end{bmatrix} \tag{4.6}$$

The disturbance rejection component also faces the limitation that disturbance must be bounded and differentiable. In terms of realizing the controller on hardware the time steps used when performing the required analog to digital conversions must be small enough such that the corresponding analog signal remains differentiable in the digital domain. Furthermore, the LADRC parameters must be selected such that the control signal is realizable by the hardware system. For example, if the hardware is incapable of generating a control signal because its magnitude is too great, the controller will not function as intended and hence, the system will not be controlled.

The parameters obtained through the parameter estimation algorithm will be used to simulate the closed loop system behaviour in Simulink. Performing a software simulation confirms whether the control signal is realizable. However, this does not imply that the simulation result and the experimental result are identical because there are noise factors and other disturbances that are small and difficult or even impossible to predict exactly. To demonstrate the purpose of software simulation, a scenario in which controller saturation occurs and the solution to this problem ensues.

The tracking of the experiment on the P-753 1.CD are shown in Fig. 4.1. It is

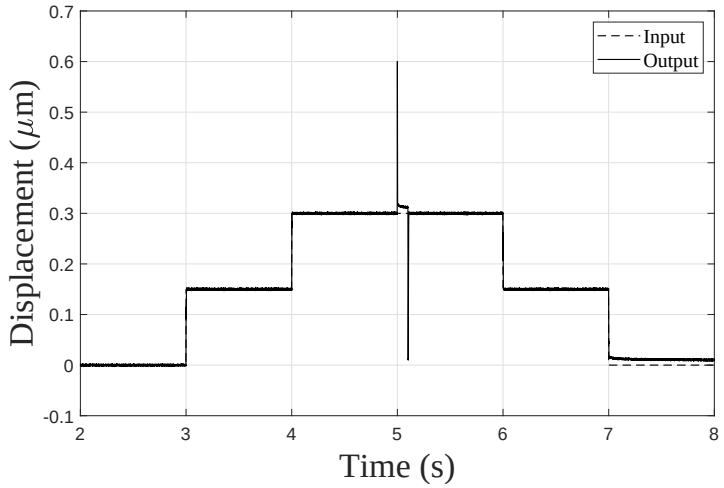

(a) Input vs Output

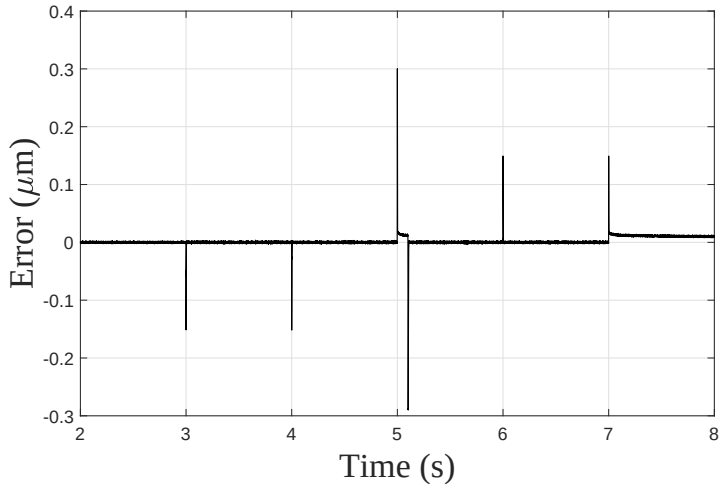

(b) Error

Figure 4.1: P-753 1.CD motion tracking when control signal is saturated

evident from these two figures that after 7 s, the error is decreasing at a slower rate in comparison to the settling between 6 and 7 seconds. The reason for this is explained when the control signal shown in Fig. 4.2 is examined.

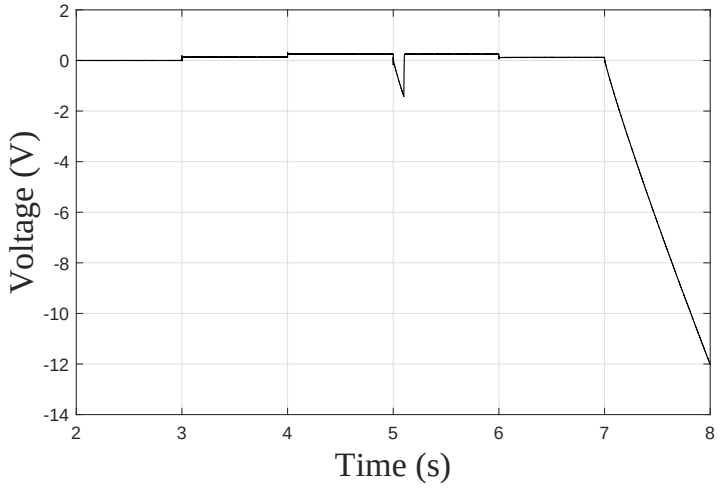

Figure 4.2: Example of saturated control signal used to control P-753 1.CD which generated Fig. 4.1

The control signal goes below zero twice. The control signal first goes below zero at approximately 5 seconds, the effect on the system response is not obvious since the error corrected for is small and the positive step input changes the error term. The second time however the effect of the saturation is more pronounced as the controller cannot supply the required input voltage required to drive the system to the desired trajectory and another positive voltage offset was not added. This issue can be resolved by adding a constant positive voltage bias to the input signal, permitting the controller to apply a larger negative voltage signal to drive the system to the desired trajectory as can be seen in Fig. 4.3.

The parameters to control the single PEA using LADRC under sinusoidal reference inputs of different frequencies were obtained using the Taguchi's method. The fitness function used for the optimization, is the percent relative ITAE as mentioned in Section 3.1. Thus the relative percentage error of the system response was calculated with respect to the input tracking trajectory. A parameter set was accepted if it

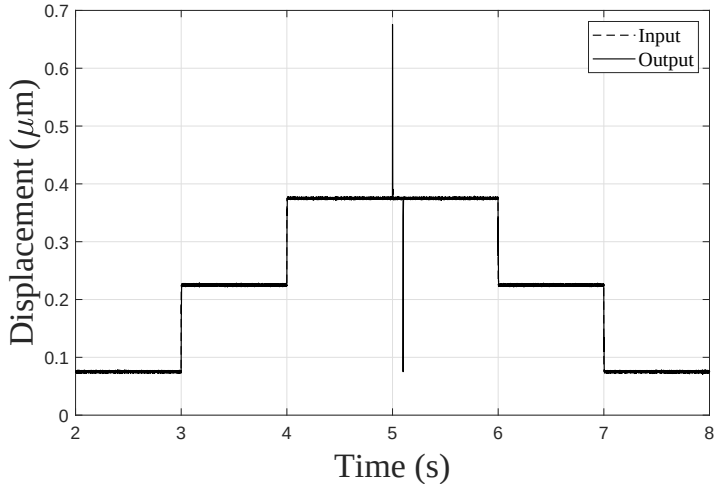

(a) Input vs Output

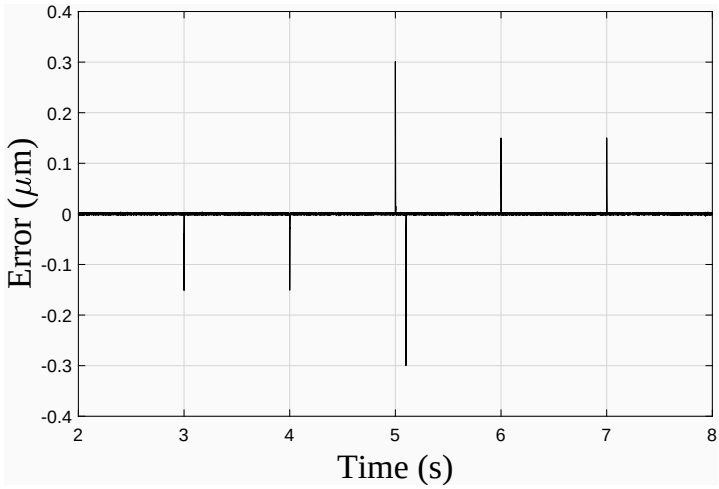

(b) Error

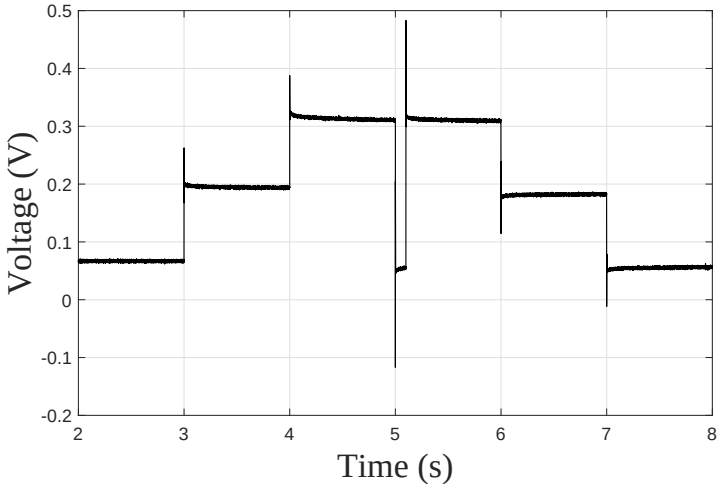

(c) Control signal

Figure 4.3: P-753 1.CD motion tracking with nonzero input bias

Table 4.1: Phase difference between input sinusoidal signal and closed loop response of single PEA with LADRC.

Frequency of Input Signal	Phase Difference (degrees)
20	6.7
50	9.3
100	15.68

resulted in a relative percentage ITAE less than 5%. A 0.1 V pulse that lasts for 0.1 s is input into the system at time 5 s as a disturbance to confirm that the control system can indeed correct for disturbances. The numerical value of 5% serves as a target for the parameter estimation algorithm to converge to. The objective of controlling the PEA for sinusoidal inputs is to determine the closed loop systems behaviour as the frequency of the input signal increases. The results can be seen in Figs. 4.4 - 4.6. The fitness values associated with results of are as follows: 11.83% for the 20 Hz Sinusoidal signal, 16.24% for the 50 Hz sinusoidal signal and 27.27% for the 100 Hz sinusoidal signal and in all three cases the disturbances were successfully rejected. By examining the mini plots in Figs. 4.4 - 4.6 it can be seen that there exists a phase difference between the input and the output signal. The phase differences between the input signal and the closed loop system response are shown in Table 4.1.

4.1 Addition of Feedforward Compensators

Table 4.1 indicates that the phase difference increases as the frequency of the input signal increases. The phase shift is compensated for with the addition of feedforward compensators. The compensators are all pass filters and have transfer functions of the following form:

$$\frac{\alpha(s-N)}{s+N} \tag{4.7}$$

where α is the steady state gain and N is a number used to shift the phase of the input signal

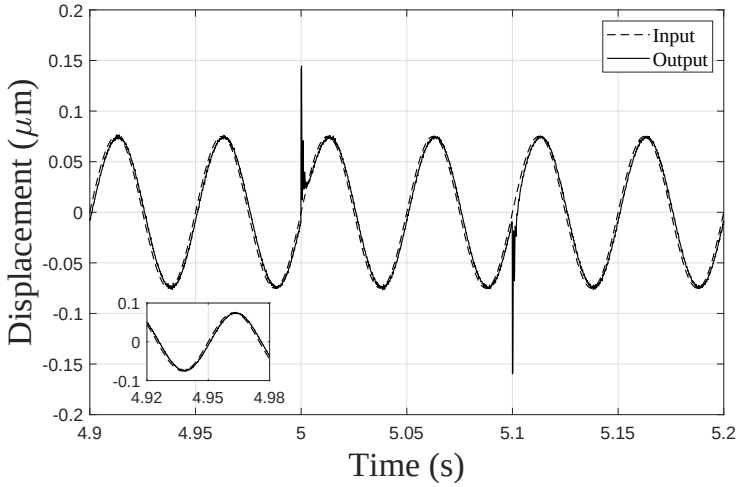

(a) 20 Hz sinusoidal tracking signal

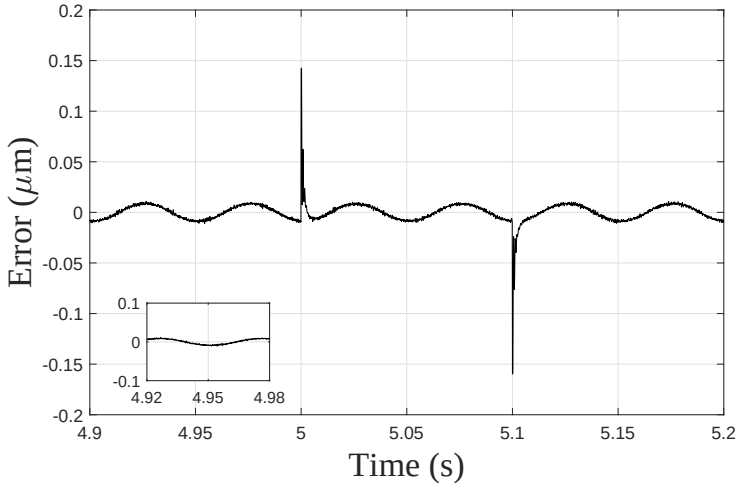

(b) 20 Hz sinusoidal tracking error

Figure 4.4: Response of the single PEA with LADRC to 0.05 V 20 Hz sinusoidal signal with disturbances at 5 s (0.1 V) and 5.1 s (-0.1 V)

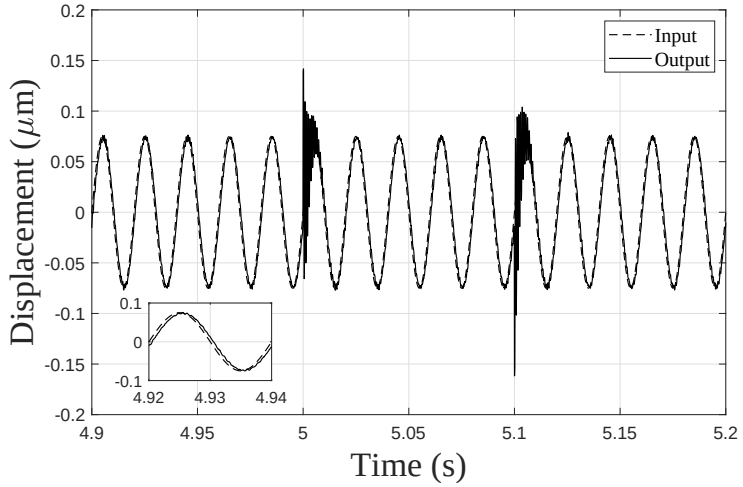

(a) 50 Hz sinusoidal tracking signal

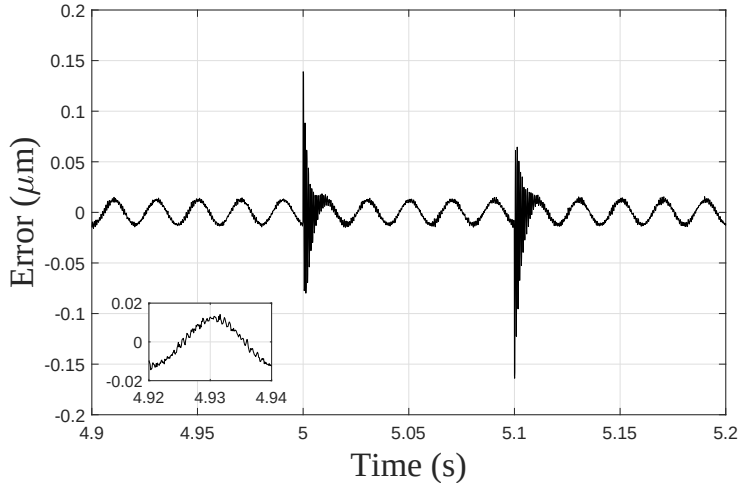

(b) 50 Hz sinusoidal tracking error

Figure 4.5: Response of the single PEA with LADRC to 0.05 V 50 Hz sinusoidal signal with disturbances at 5 s (0.1 V) and 5.1 s (-0.1 V)

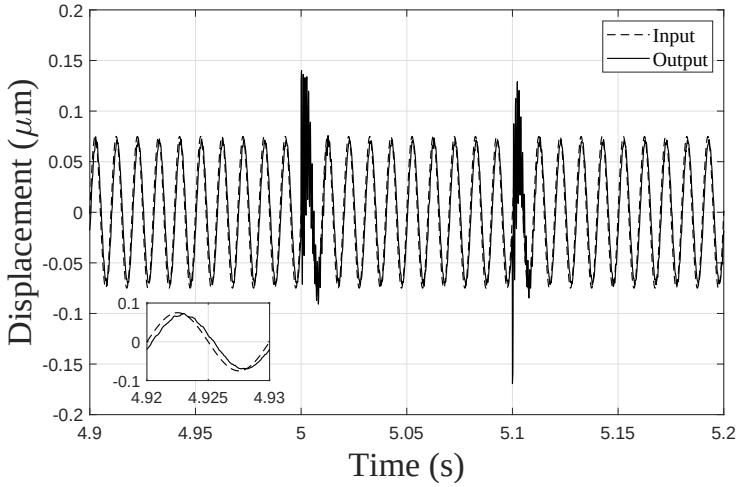

(a) 100 Hz sinusoidal tracking signal

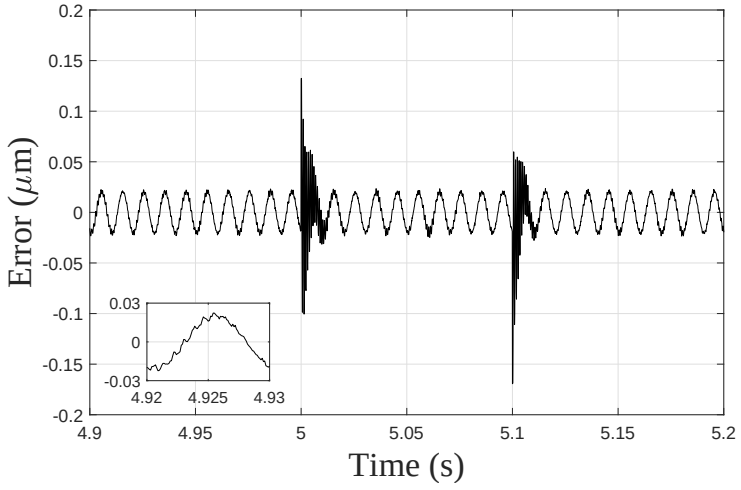

(b) 100 Hz sinusoidal tracking error

Figure 4.6: Response of the single PEA with LADRC to 0.05 V 100 Hz sinusoidal with disturbances at 5 s (0.1 V) and 5.1 s (-0.1 V)

To determine N and α, the system response without the feedforward compensator is obtained first. The phase difference between the output signal and the reference input is calculated by obtaining of the FFTs of the output and input signal and computing the phase angle between the frequencies of interest. The sinusoidal reference inputs only have one frequency. In the event a reference input with multiple frequencies is used, then the phase angles at multiple frequencies must be considered. Specifying the frequencies of interest avoids contamination from the noise. For example, if the phase difference was determined by eye, the noise superimposed on the output signal creates an error in the estimation of the phase. Computing the phase angle at only the frequency of interest avoids the discrepancies introduced by other frequency components. The corresponding value for N is calculated from the transfer function.

$$\angle phase = \tan^{-1} \frac{2N\omega}{(\omega^2 - N^2)} \tag{4.8}$$

The magnitude of this feedforward compensator without α is one. By multiplying the feedforward compensator by alpha introduces a constant gain of magnitude α. The value of α is obtained by computing the mean of the output peaks divided by the mean of the input peaks. The computed α and N are tried in the hardware simulation and the results are as shown in Figs. 4.7 - 4.9. From visual inspection of the graphs alone, an improvement in tracking is evident. The new fitness values associated with results of are as follows: 1.61% for the 20 Hz sinusoidal signal, 2.92% for the 50 Hz sinusoidal signal and 3.78% for the 100 Hz sinusoidal signal. The fitness values achieved both before and after the inclusion of the feedforward compensators are provided in Table 4.2 to display the numerical improvement in the tracking of the desired signal when the feedforward compensator is included.

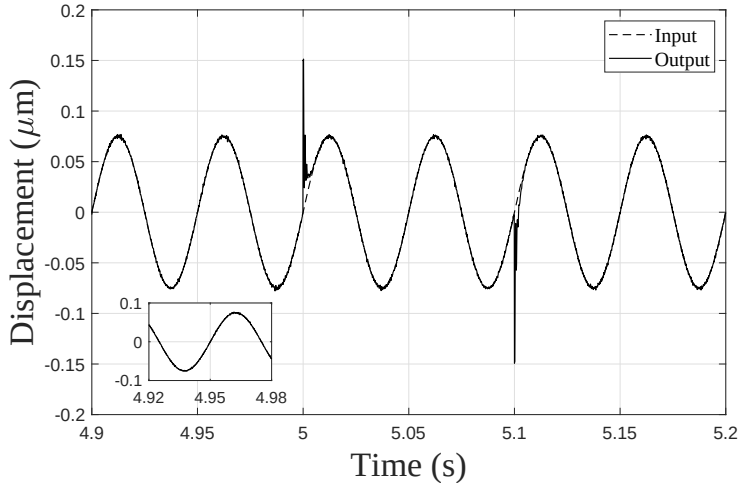

(a) 20 Hz sinusoidal tracking signal

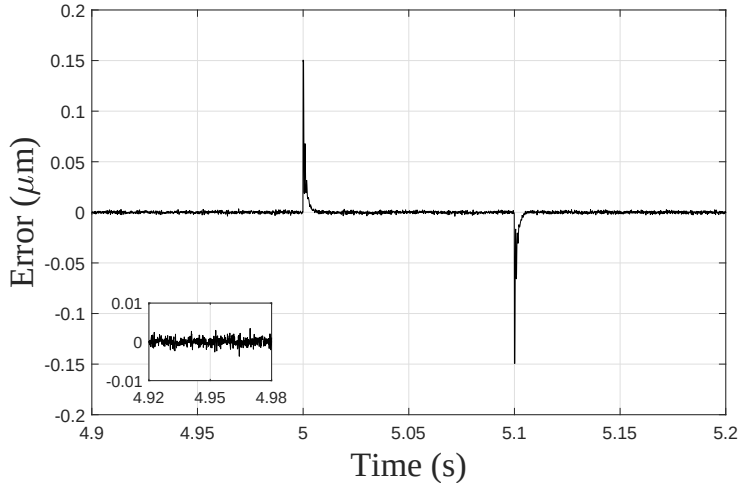

(b) 20 Hz sinusoidal tracking error

Figure 4.7: Response of the single PEA with the feedforward compensator and LADRC to 0.05 V 20 Hz sinusoidal signal with disturbances at 5 s (0.1 V) and 5.1 s (-0.1 V)

Table 4.2: Relative percentage ITAE fitness comparison between LADRC without feedforward compensators and with feedforward compensators

Sinusoidal Reference Input Signal / **Number of Feedforward Compensators**	**20 Hz**	**50 Hz**	**100 Hz**
0	11.8	16.2	27.3
1	1.6	2.9	3.8

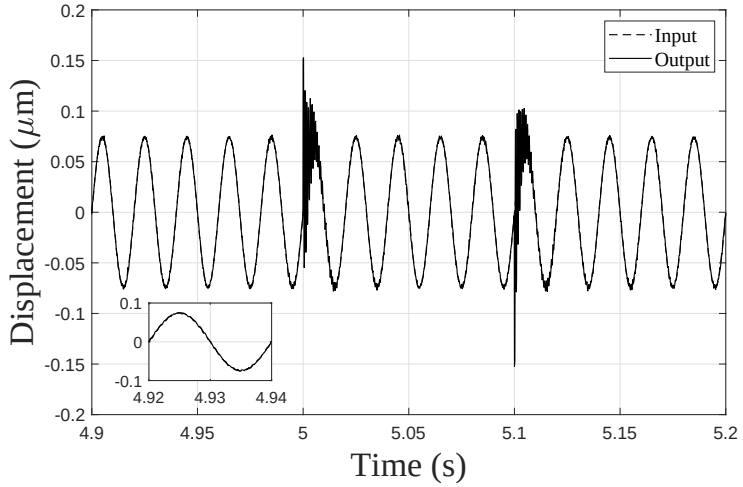

(a) 50 Hz sinusoidal tracking signal

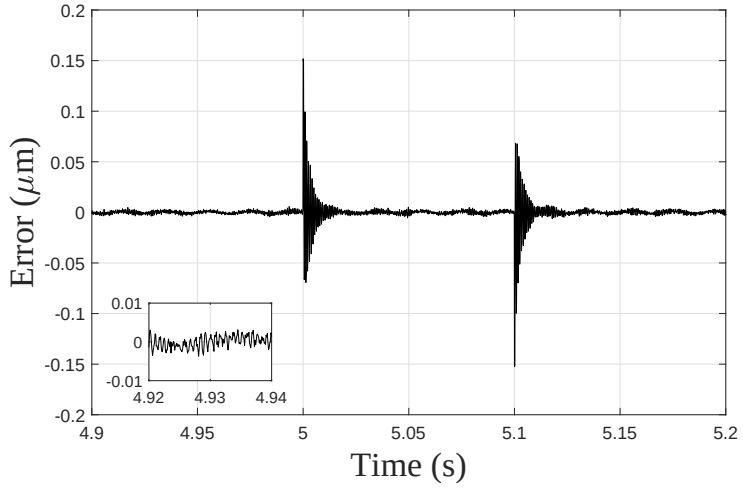

(b) 50 Hz sinusoidal tracking error

Figure 4.8: Response of the single PEA with the feedforward compensator and LADRC to 0.05 V 50 Hz sinusoidal signal with disturbances at 5 s (0.1 V) and 5.1 s (-0.1 V)

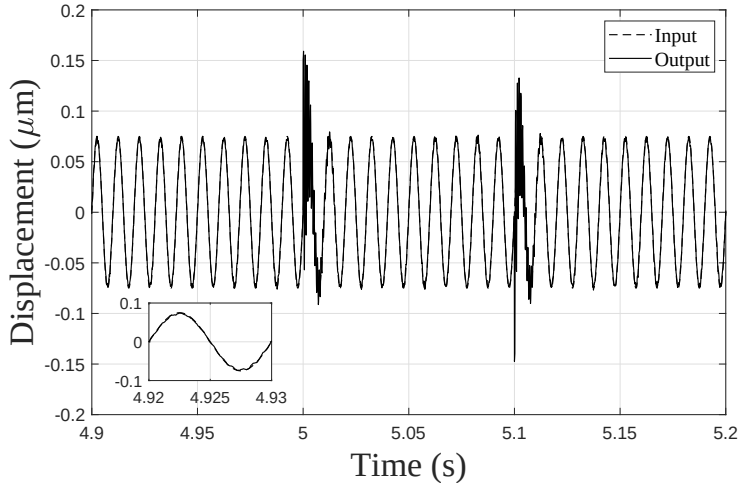

(a) 100 Hz sinusoidal tracking signal

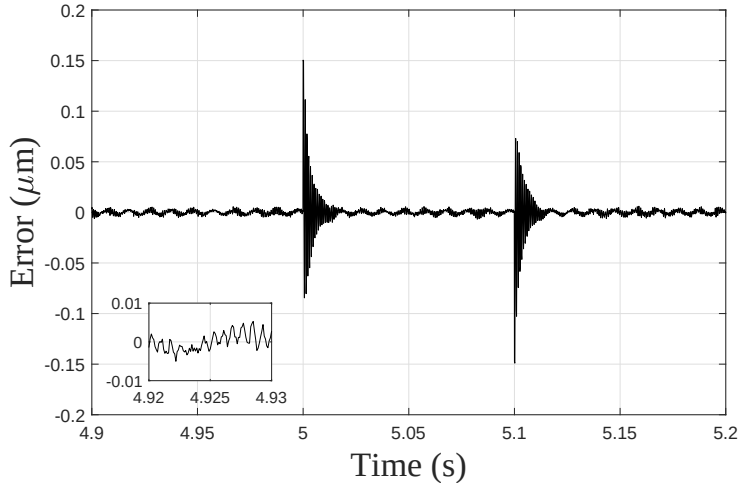

(b) 100 Hz sinusoid tracking error

Figure 4.9: Response of the single PEA with the feedforward compensator and LADRC to 0.05 V 100 Hz sinusoidal signal with disturbances at 5 s (0.1 V) and 5.1 s (-0.1 V)

4.2 Robustness to Process Perturbations

The primary advantage of LADRC is in its ability to control a system with minimal information regarding the plant. However it is important to verify that the designed controller does exhibit this robustness property. This can be demonstrated by measuring the controllers sensitivity to process perturbations.

Recall the single PEA plant shown in Eqn.(2.1) as $Gp = \frac{-3348s^2+3.572\times10^7}{s+1.233\times10^4 s+5.041\times10^7}$. Select $w_0 = 1 \times 10^4$, $kp = 1 \times 10^8$, $kd = 2 \times 10^4$ and $b_0 = 3.572 \times 10^7$. The loop gain transfer function of the controller and the plant is shown in Fig. 4.10 and the transfer function derivation is provided in Appendix A.

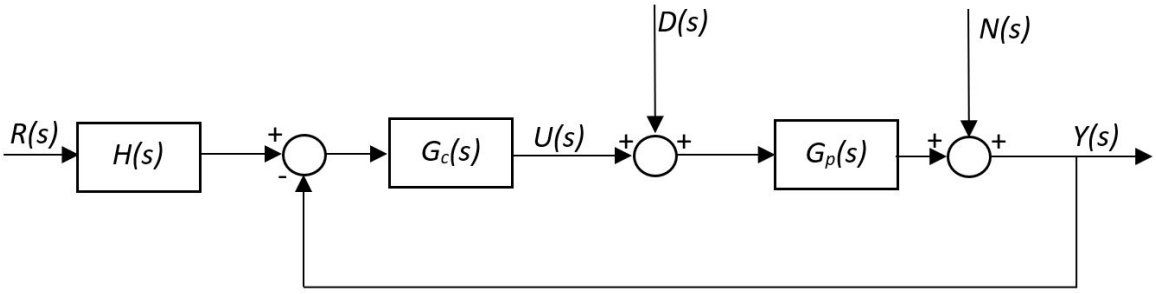

Figure 4.10: System 2 Degree of Freedom (DOF) block diagram of LADRC [4]. The diagram contains the frequency domain representation of the system. $R(s)$ is the input signal, $H(s)$ is the feedforward component, $U(s)$ is the control signal, $Y(s)$ is measured output signal, G_c is the controller, G_p is the plant, $D(s)$ is the disturbance signal (containing unknown plant dynamics and load disturbances) and N(s) is the noise (external disturbance).

The system error is expressed as

$$E = HR - Y \tag{4.9}$$

where

$$Y = G_c G_p(HR - Y) + G_p D + N \tag{4.10}$$

$$Y = \frac{G_c G_p(HR) + G_p D + N}{G_c G_p + 1} \tag{4.11}$$

where $L = G_c G_p$ is referred to as the loop gain transfer function.

$$Y = THR + SG_pD + SN \tag{4.12}$$

where $T = \frac{G_cG_p}{G_cG_p+1}$ is the complementary sensitivity transfer function and $S = \frac{1}{G_cG_p+1}$ is the sensitivity transfer function. The error is simplified to

$$E = HR - THR + SG_pD + SN \tag{4.13}$$

$$E = HR(1 - T) - SG_pD - SN \tag{4.14}$$

$$E = HRS - SG_pD - SN \tag{4.15}$$

Note that the transition from Eq. (4.14) to Eq. (4.15), is because $S + T = 1$. The control system is designed so that there is small tracking error in the system response, therefore S should be small. The bode plot shown in Fig. (4.11) demonstrates that the Sensitivity is small for the system, however as seen from the bode plot the sensitivity increases past approximately 6,000 $\frac{rad}{s}$. This implies that the system is sensitive to high frequency components. However this is not of great concern as seen from the open loop transfer functions bode plot provided in, Fig. fig:singlePEAbodePlot), the -3 dB cutoff frequency response of the system is before 6,000 $\frac{rad}{s}$. Sensitivity to perturbation increase as distance between the Nyquist critical point -1 and the open loop transfer function evaluated at a specific frequency decreases [36].

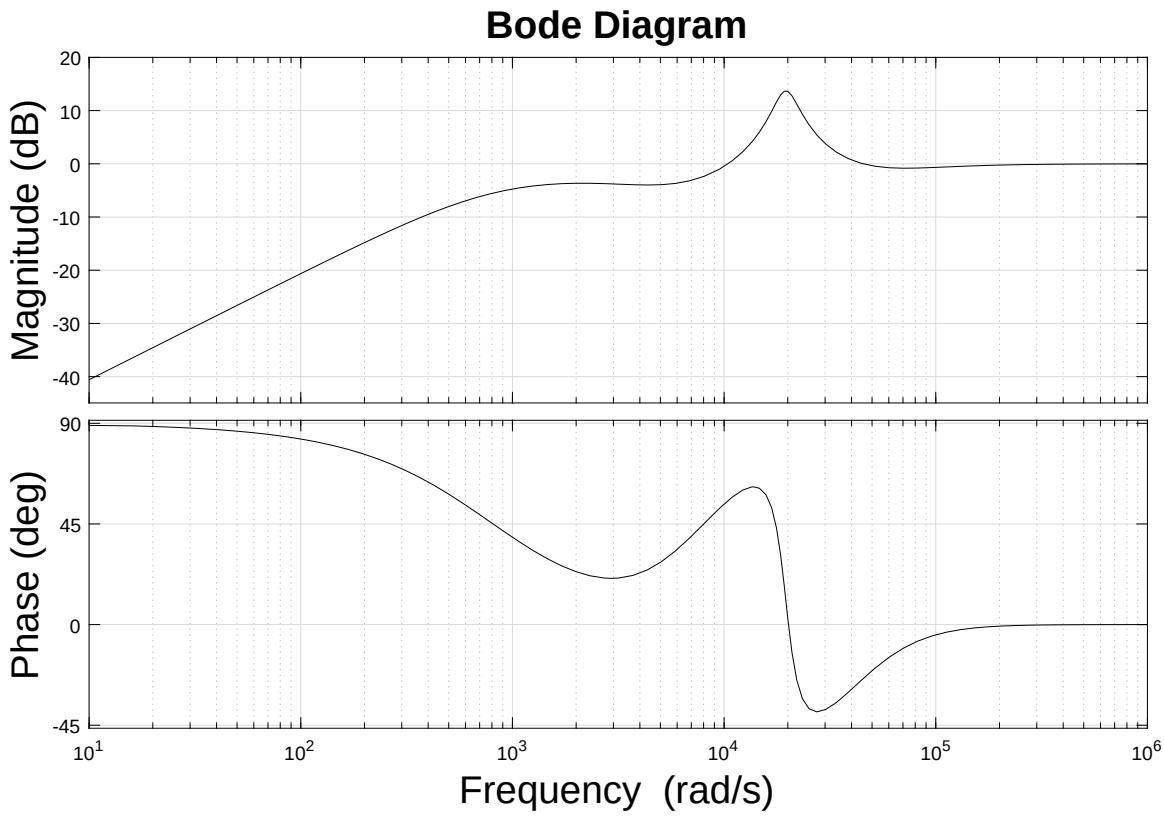

Figure 4.11: Sensitivity plot of single PEA system with LADRC

Chapter 5

Synchronized Control of Three PEAs in Parallel Installation using LADRC

Motivation for this research comes from the three PEAs in parallel installation used to control the gap spacing of the Fabry-Pérot Spectrometer. The gap spacing is controlled at the nanometer level to achieve wavelength scanning in order for the Fabry-Pérot to transmit at selected frequencies. The gap spacing is adjusted by three PEAs moving a mirror in linear motion.

The Fabry-Pérot Spectrometer is given step signals as commands to adjust the gap spacing between its mirrors. For this input, synchronous steady state motion is desired, since the images are taken at the end of the transient response. Synchronous steady state motion is achieved when all three PEAs achieve the same displacement. In practice all three PEAs will not be in perfect synchronization due to capacitor resolution limits and noise. For this research synchronous steady state motion is achieved when all three PEAs have achieved a tracking error that is ± 0.2 % for a reference input of 0.5 μm. These values are selected so that a greater steady state

accuracy for the mirror gap spacing can be achieved by the PEAs than during the Alice Springs balloon flight. Synchronization of the transient is also desired, because this ensures that the three PEAs reach steady state at the same time. Hence the user will not have to wait for the PEAs to achieve steady state one at a time.

The synchronous LADRC involves a Multi Input Multi Output (MIMO) LADRC controlling the error for each of the PEA and a synchronous controller that extracts the decoupled synchronous error, which is the difference in position between each of the PEAs. The coupling is due to mechanical coupling between the plate and the actuators. A weight term, G_{synch}, is used to scale the synchronous coupling error, TE, such that the coupling error is controlled by a simple proportional feedback controller. This is done while taking into consideration that the combined LADRC and synchronization feedback control signal is within the hardware operating voltage of the system and is therefore realizable. The combined control signal is then fed into the hardware system. A mathematical representation of this process can also be seen through the following equations [2, 37–39]:

$$E = \begin{bmatrix} e_1 \\ e_2 \\ e_3 \end{bmatrix}$$

where $e_1 = r$ - y_1, $e_2 = r$ - y_2, $e_3 = r$ - y_3, e is the error, r is the input signal to the three PEA system and y is the output of the three PEA system.

$$T = \begin{bmatrix} 2 & -1 & -1 \\ -1 & 2 & -1 \\ -1 & -1 & 2 \end{bmatrix}$$

$$TE = \begin{bmatrix} (y_2 - y_1) + (y_3 - y_1) \\ (y_1 - y_2) + (y_3 - y_2) \\ (y_1 - y_3) + (y_2 - y_3) \end{bmatrix}$$

$$u_{synch} = T(y - r \begin{bmatrix} 1 \\ 1 \\ 1 \end{bmatrix}) G_{synch} \tag{5.1}$$

$$u = u_{LADRC} + u_{synch} \tag{5.2}$$

Eqs. (5.1-5.2) describe the LADRC with the synchronization term. However, it

is important to verify that the synchronized component has an impact in the system response. This can be done by comparing the system response with the synchronization component, Fig. 5.4, to without the synchronization component, Fig. 5.5, when all the other parameters are kept the same. The result of the comparison is shown in Fig. 5.6. The synchronization error when the synchronization component is included, Fig. 5.6(a), is lower than when it is not, Fig. 5.6(b). This analysis demonstrates that inclusion of the synchronization component reduces the synchronization error in the system response.

The parameters for the three PEA system are obtained using the Taguchi's method due to the reasons addressed in Section 3.6. It proved to be the most reliable and quick optimization algorithm, compared to the Genetic Algorithm and Brute-force method. The fitness function used for optimization consists of dividing the ITAE of the error with the ITAE of the input signal and a constant zero amplitude signal and then converting the result to a percentage, refer to Eq. (3.2). Thus the relative percentage ITAE of the system response was calculated with respect to the input signal. The results shown in Figs. 5.1 - 5.3 demonstrate that there is a phase offset as the frequency of the input signal increases. The three PEA system was further excited with disturbances of different magnitudes and at different times to each PEA to demonstrate that each disturbance is rejected. The fitness values associated with signals of different frequencies are as follows: 103.7% for the 20 Hz sinusoidal signal, 133.5% for the 50 Hz sinusoidal signal and 231.4% for the 100 Hz sinusoidal signal. Close inspection of the graphs indicate that these errors are large because of the existing phase difference between the input signal and the output system response.

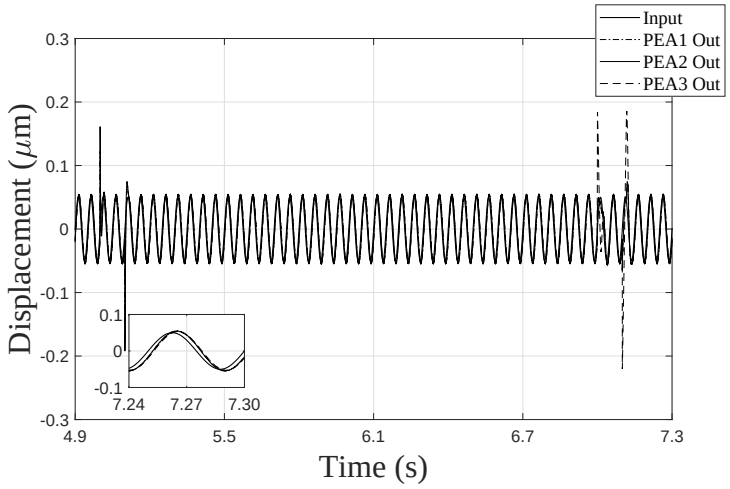

(a) 20 Hz sinusoidal tracking signal

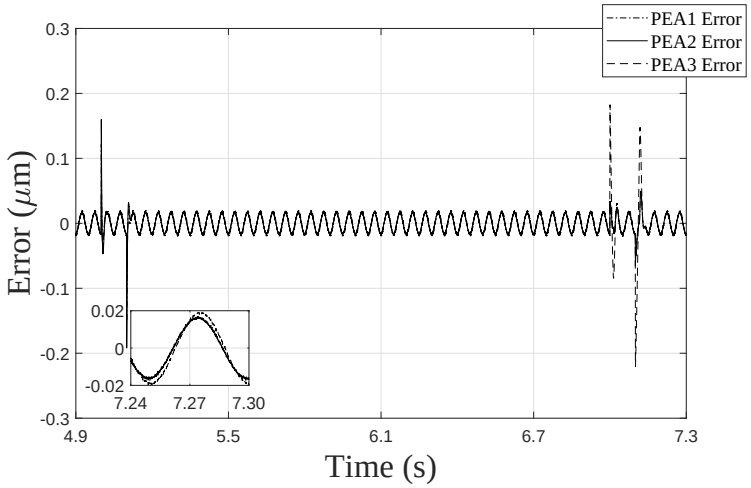

(b) 20 Hz sinusoidal tracking error

Figure 5.1: Response of three PEA system with LADRC to 0.05 V 20 Hz sinusoidal signal with disturbances at 5 s (0.1 V) and 5.1 s (-0.1 V) for PEA 1, at 5 s (0.15 V) and 5.1 s (-0.15 V) for PEA 2 and at 7 s (0.2 V) and 7.1 s (-0.2 V) for PEA 3

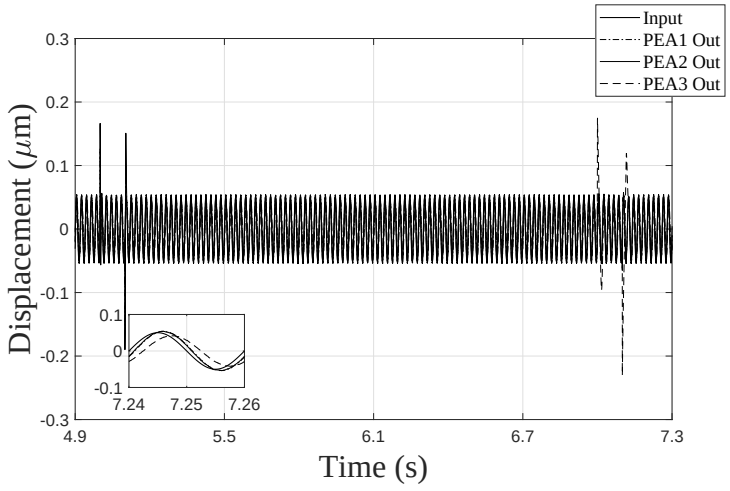

(a) 50 Hz sinusoidal tracking signal

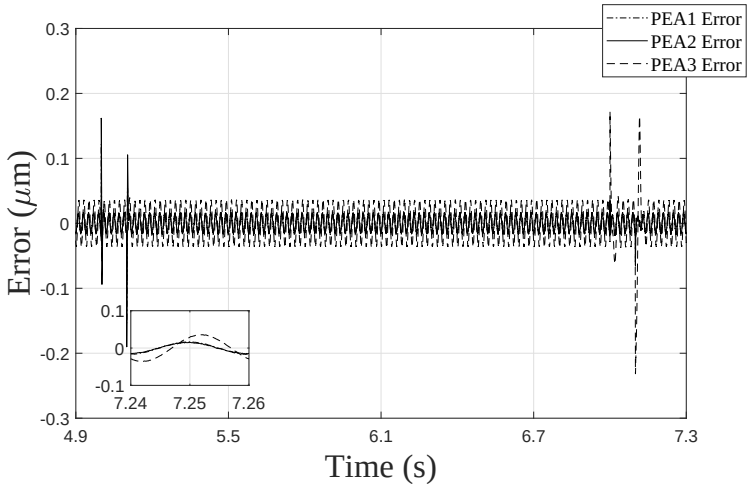

(b) 50 Hz sinusoidal tracking error

Figure 5.2: Response of three PEA system with LADRC to 0.05 V 50 Hz sinusoidal signal with disturbances at 5 s (0.1 V) and 5.1 s (-0.1 V) for PEA 1, at 5 s (0.15 V) and 5.1 s (-0.15 V) for PEA 2 and at 7 s (0.2 V) and 7.1 s (-0.2 V) for PEA 3

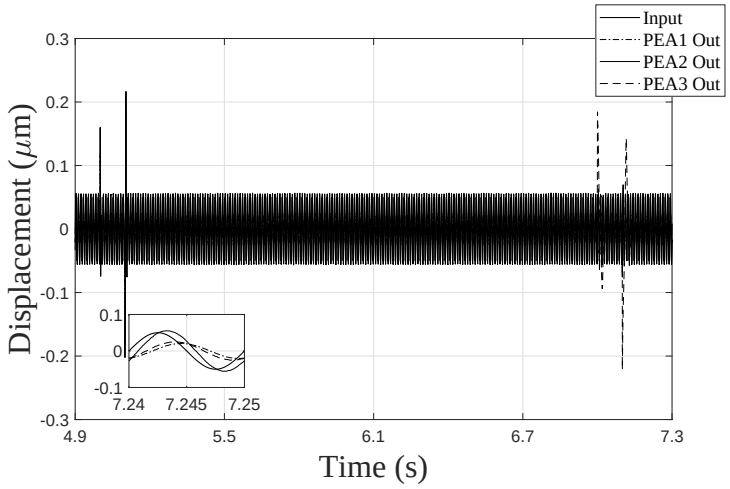

(a) 100 Hz sinusoidal tracking signal

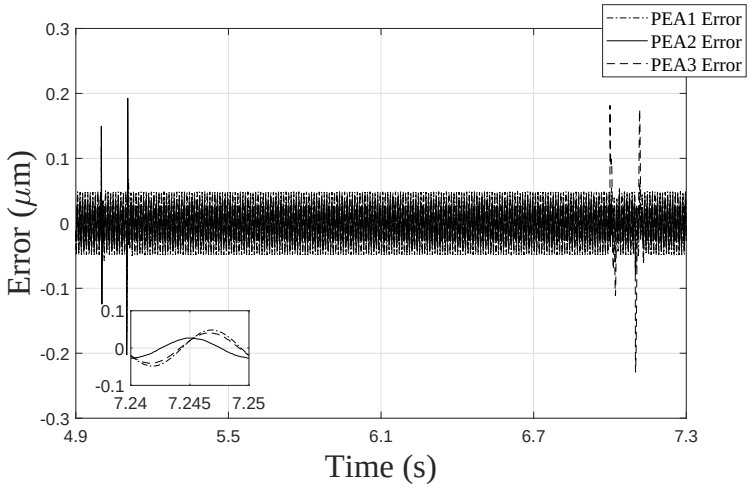

(b) 100 Hz sinusoidal tracking error

Figure 5.3: Response of three PEA System With LADRC to 0.05 V 100 Hz sinusoidal signal with disturbances at 5 s (0.1 V) and 5.1 s (-0.1 V) for PEA 1, at 5 s (0.15 V) and 5.1 s (-0.15 V) for PEA 2 and at 7 s (0.2 V) and 7.1 s (-0.2 V) for PEA 3

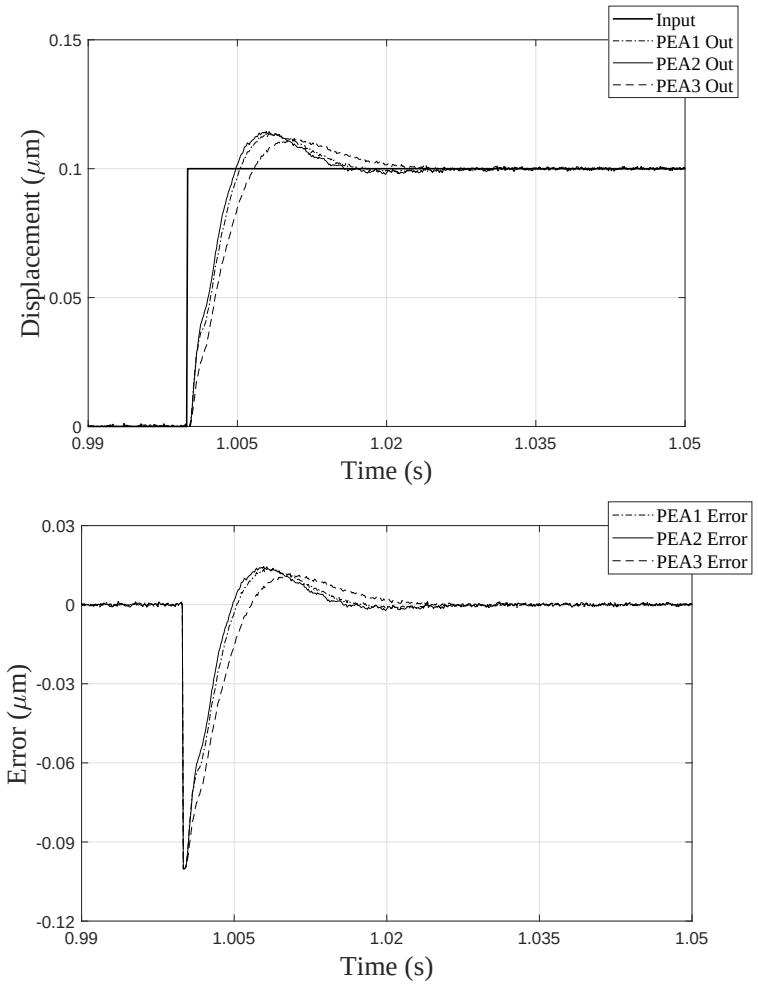

Figure 5.4: Closed loop step response and error for LADRC with synchronization

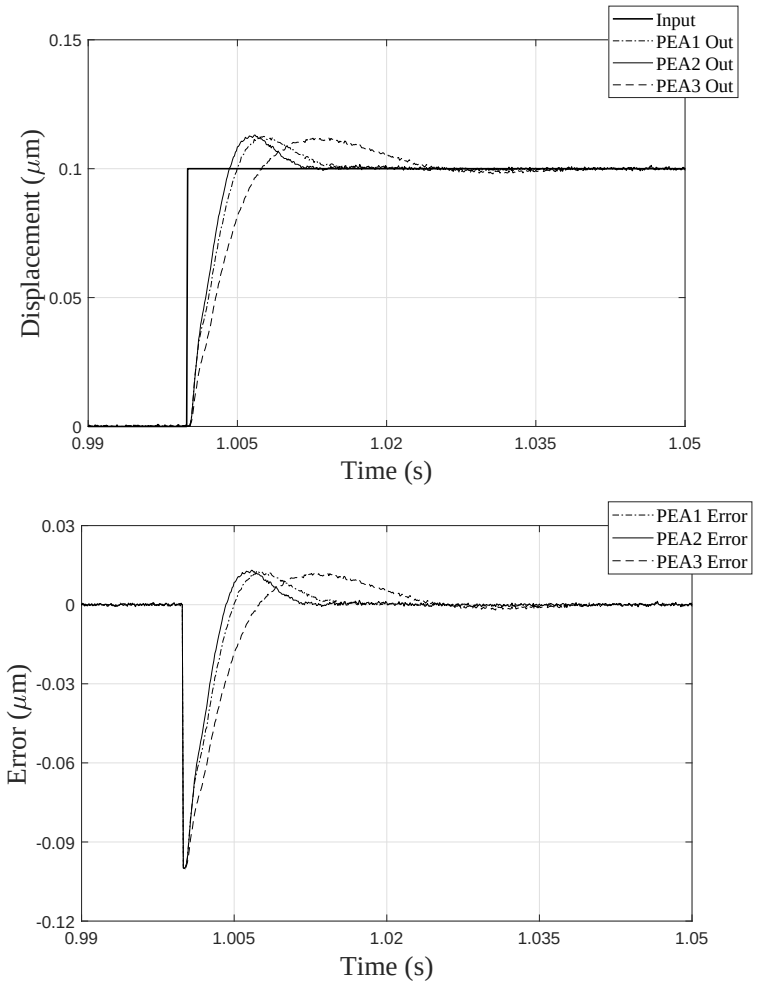

Figure 5.5: Closed loop step response and error for LADRC without synchronization

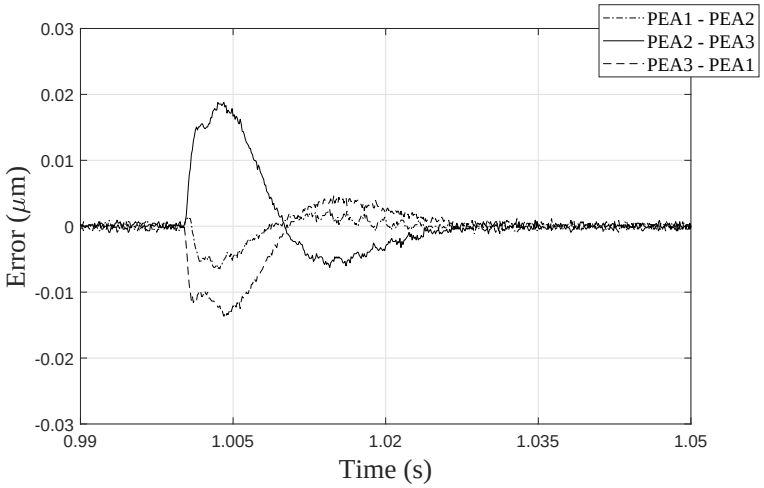

(a) With synchronization

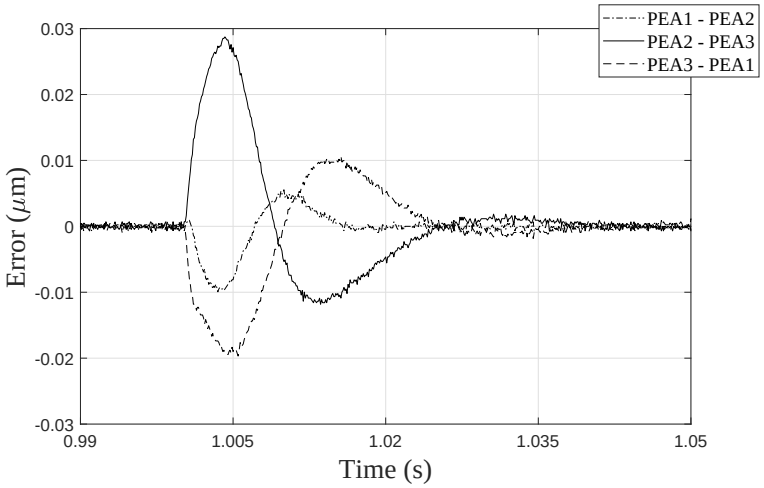

(b) Without synchronization

Figure 5.6: Synchronization error of closed loop step response for LADRC

5.1 Addition of Feedforward Compensators

When designed well the LESO reduces the plant to that of an cascaded integrator as discussed in Section 1.2. However in practice, the implementation of the LESO is not perfect and there are magnitude and phase offsets. To compensate for these offsets, the addition of feedforward compensators are investigated. The control performance is improved with the addition of feedforward compensators as shown in Figs. 5.7 - 5.11. The feedforward compensators are of the same structure as with the single PEA case, refer to Eq. (4.7). In this case with three PEAs, each PEA input has its own compensator, determined through the same methods as was done for the single PEA case in Section 4.1. However unlike the setup with the single PEA, the existence of the coupling between three PEAs add complexity with regards to designing the feedforward compensators. In the case of 50 Hz and 100 Hz sinusoidal input signals, two cascaded feedforward compensators are required to achieve a combined fitness value below 15% for the three PEAs as shown in Figs. 5.9 and 5.11. Once the first feedforward compensator is determined, the output is used to determine the second compensator. The addition of just one feedforward compensator, however, reduced the fitness values to: 4.6% for the 20 Hz sinusoidal signal, 27.0% for the 50 Hz sinusoidal signal and 33.5% for the 100 Hz sinusoidal signal. With two cascaded feedforward compensators the fitness values were reduced to 7.0% for the 50 Hz sinusoidal signal and 14.8% for the 100 Hz sinusoidal signal. Table 5.1 displays the relative percentage ITAEs of the three PEA system without feedforward compensators, with 1 feedforward compensator and with 2 feedforward compensators. The decrease in the relative percentage ITAE with the inclusion of feedforward compensators confirm that the feedforward compensators are a viable solution to correcting the low pass filter effect introduced by the LADRC into the control system.

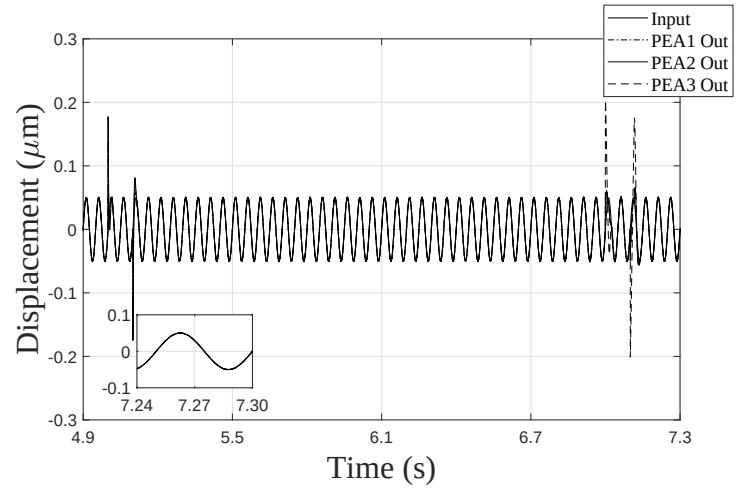

(a) 20 Hz sinusoidal tracking signal

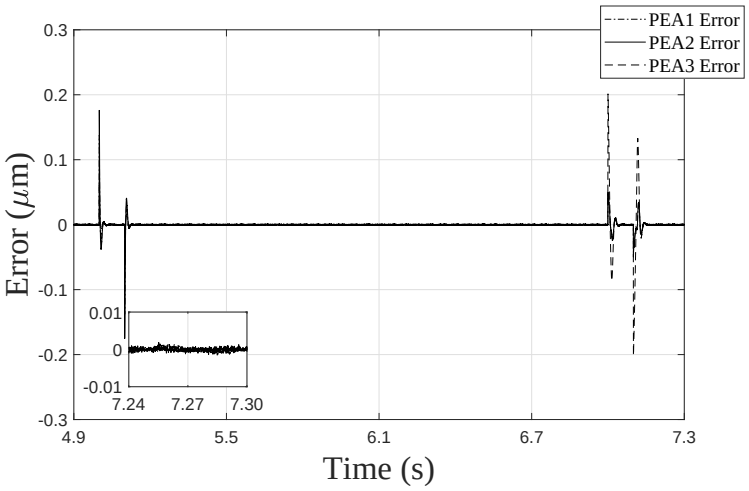

(b) 20 Hz sinusoidal tracking error

Figure 5.7: Response of three PEA system with feedforward compensators and LADRC to 0.05 V 20 Hz sinusoidal signal with disturbances at 5 s (0.1 V) and 5.1 s (-0.1 V) for PEA 1, at 5 s (0.15 V) and 5.1 s (-0.15 V) for PEA 2 and at 7 s (0.2 V) and 7.1 s (-0.2 V) for PEA 3

Table 5.1: Relative percentage ITAE fitness comparison between synchronized LADRC without feedforward compensators and with feedforward compensators

Sinusoidal Reference Input Signal / **Number of Feedforward Compensators**	**20 Hz**	**50 Hz**	**100 Hz**
0	103.7	133.5	231.4
1	4.6	27.0	33.5
2	-	7.0	14.8

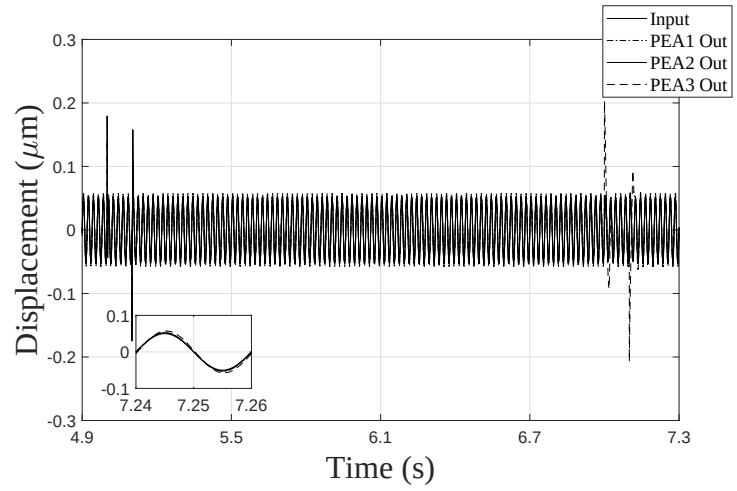

(a) 50 Hz sinusoidal tracking signal

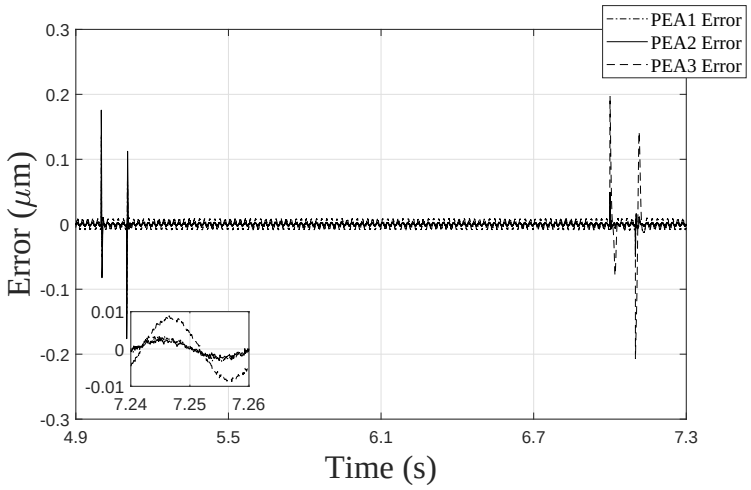

(b) 50 Hz sinusoidal tracking error

Figure 5.8: Response of three PEA system with feedforward compensators and LADRC to 0.05 V 50 Hz sinusoidal signal with disturbances at 5 s (0.1 V) and 5.1 s (-0.1 V) for PEA 1, at 5 s (0.15 V) and 5.1 s (-0.15 V) for PEA 2 and at 7 s (0.2 V) and 7.1 s (-0.2 V) for PEA 3

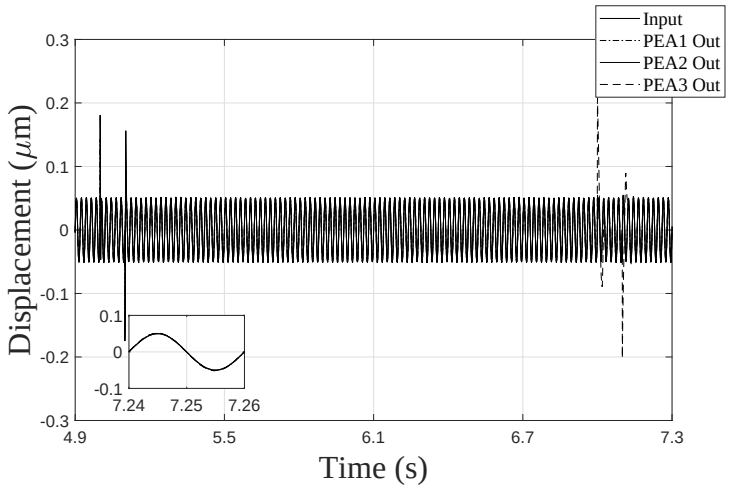

(a) 50 Hz sinusoidal tracking signal

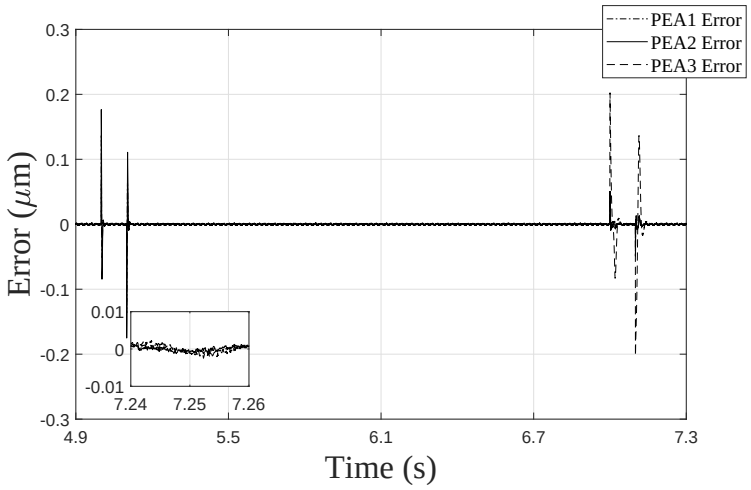

(b) 50 Hz sinusoidal tracking error

Figure 5.9: Response of three PEA system with cascaded feedforward compensators and LADRC to 0.05 V 50 Hz sinusoidal signal with disturbances at 5 s (0.1 V) and 5.1 s (-0.1 V) for PEA 1, at 5 s (0.15 V) and 5.1 s (-0.15 V) for PEA 2 and at 7 s (0.2 V) and 7.1 s (-0.2 V) for PEA 3

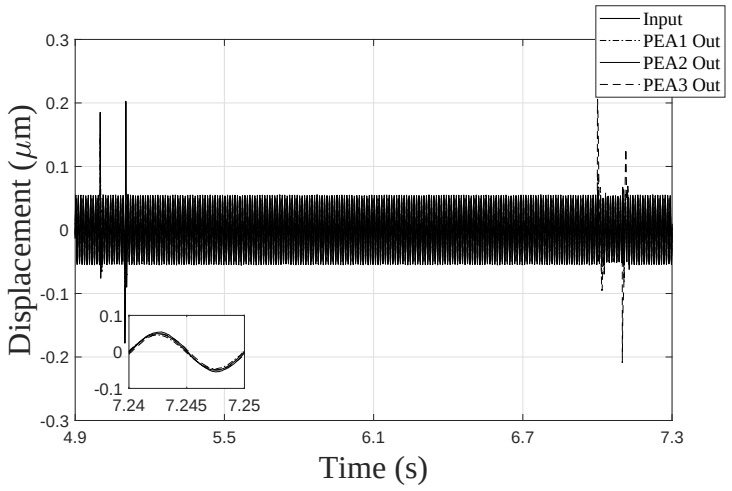

(a) 100 Hz sinusoidal tracking signal

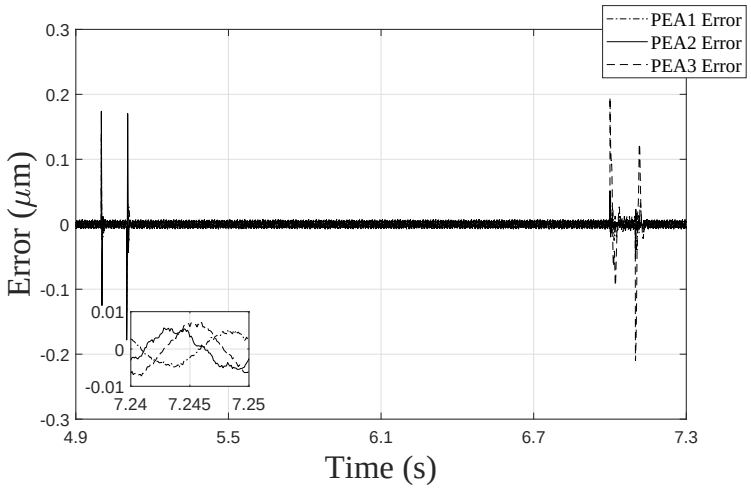

(b) 100 Hz sinusoid tracking error

Figure 5.10: Response of three PEA system with feedforward compensators and LADRC to 0.05 V 100 Hz sinusoidal signal with disturbances at 5 s (0.1 V) and 5.1 s (-0.1 V) for PEA 1, at 5 s (0.15 V) and 5.1 s (-0.15 V) for PEA 2 and at 7 s (0.2 V) and 7.1 s (-0.2 V) for PEA 3

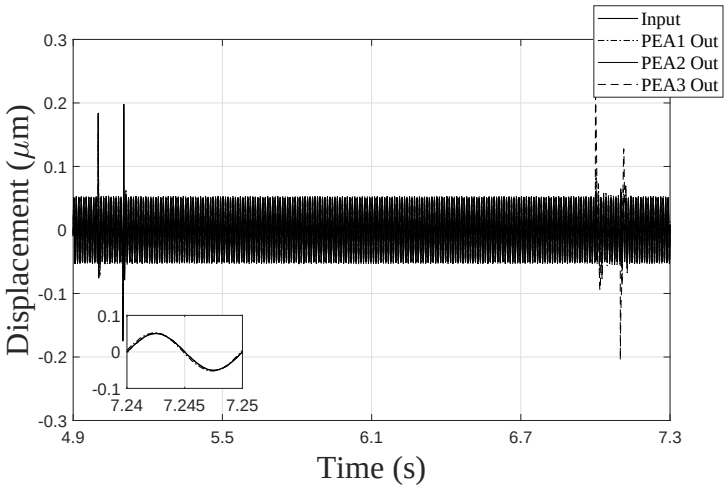

(a) 100 Hz sinusoidal tracking signal

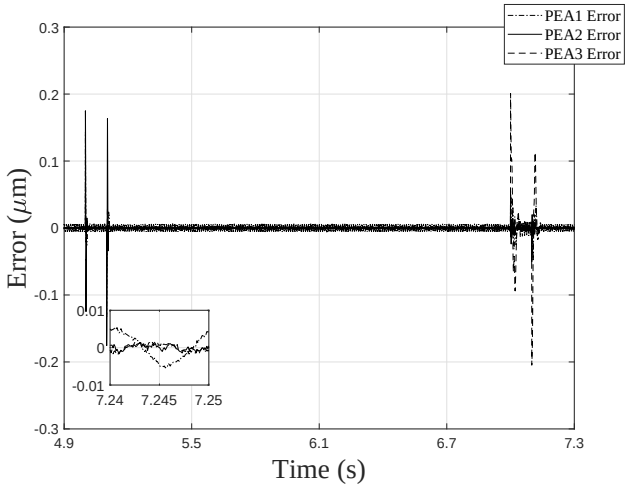

(b) 100 Hz sinusoidal tracking error

Figure 5.11: Response of three PEA system with cascaded feedforward compensators and LADRC to 0.05 V 100 Hz sinusoidal signal with disturbances at 5 s (0.1 V) and 5.1 s (-0.1 V) for PEA 1, at 5 s (0.15 V) and 5.1 s (-0.15 V) for PEA 2 and at 7 s (0.2 V) and 7.1 s (-0.2 V) for PEA 3

5.2 Synchronized LQG VS. Synchronized LADRC

Having implemented the synchronized LADRC, it is important to understand how it compares to other existing controllers. This will be done by comparing its performance to that of the synchronized LQG controller implemented on the three PEA system by Dr. Zhi Li [16].

In order to perform a fair comparison between the synchronized LADRC and the synchronized LQG, the same fitness criteria must be used. This means that the fitness function cannot be the relative percent error where ITAE is the error. The paper uses Mean Absolute Error (MAE) and Root Mean Square Error (RMSE). Furthermore the performance is evaluated by measuring the $\pm 0.2\%$ settling time and the overshoot. The synchronization matrix used in this research is the same as the matrix T2 referred to in [16]. The results of the paper indicate a 0.116 μm overshoot and a 0.162 s $\pm 0.2\%$ settling time. The synchronized LADRC was able to achieve a 0.0296 μm overshoot and a 0.0854 s $\pm 0.2\%$ settling time as shown in Fig. 5.12. Furthermore, the system response can be enhanced with the addition of low pass filters to filter out all high frequency noise components, as shown in Fig. 5.13.

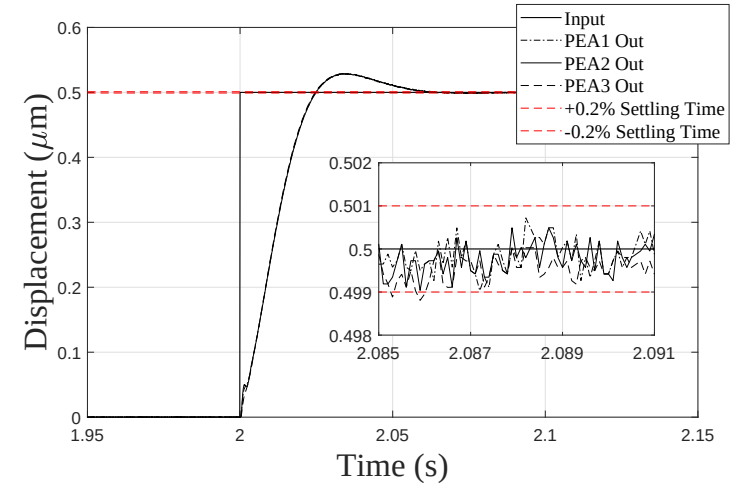

(a)

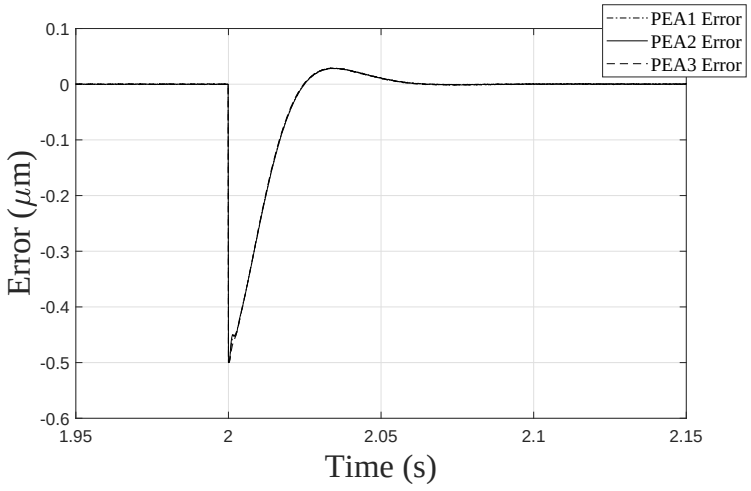

(b)

Figure 5.12: (a) LADRC best synchronization and fast tracking and (b) the tracking error.

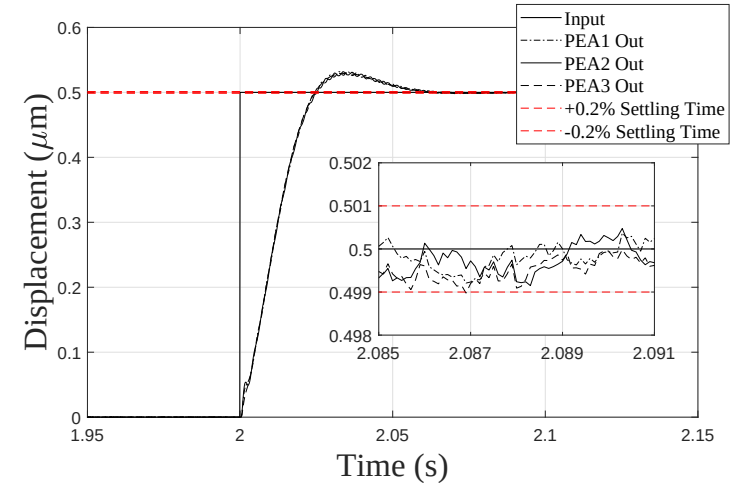

(a)

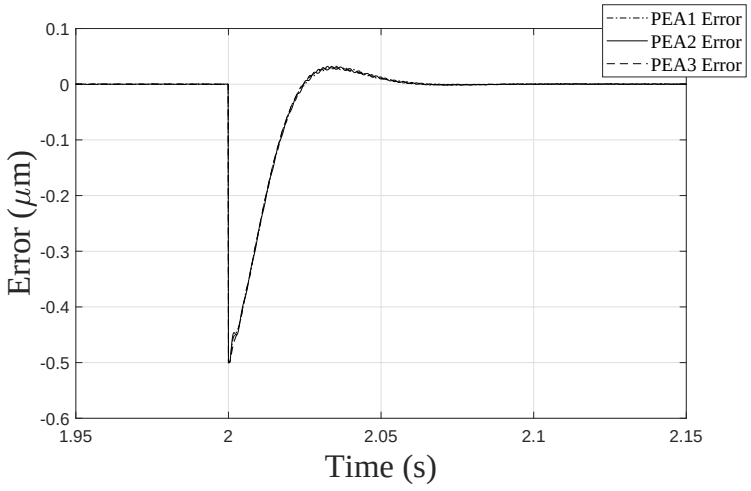

(b)

Figure 5.13: (a) LADRC best synchronization and fast tracking with low pass filter and (b) the tracking error.

Chapter 6

Conclusions and Future Work

The Fabry - Pérot spectrometer developed in the SDCNLab has been flown on stratospheric balloons to measure the albedo of ground structures and of clouds. As implied, there already exist solutions to synchronously control the three PEA system. However, these solutions require accurate modeling of the complex three PEA system. The contribution of this research is investigating the implementation of the LADRC to control a prototype three PEA system. The control parameters are selected using Taguchi's method. The LADRC is first implemented on a single PEA system and a feedforward compensator is designed to compensate for phase offsets induced by the low pass characteristics from the reduced plant. Identifying improved tracking performance from including the feedforward compensator led to adding feedforward compensators in the three PEA control system as well. The feedforward compensators are shown to improve the tracking performance of the PEAs in the three PEA system.

Synchronized LADRC displayed better results to the LQG controller designed for the same three PEA system in [16]. From this research, it has been demonstrated that a nonlinear system as complex as the three PEAs can be controlled by the LADRC. However, a limitation of this research is that the input signals are limited to be of small amplitude. The reason being that nonlinear characteristics are stronger over

a wider range of amplitude [40]. This causes the controller to be saturated without much variation in amplitude. It would be interesting to see a control solution where a model independent controller implements the synchronization strategy to control the PEA for any input voltage within the hardware limits for a wide band of frequencies. In the future, it would be interesting to see how well the LADRC performs as the actual controller for the three PEA system in a working Fabry-Pérot system rather than the prototype.

The applications of PEAs are not limited to controlling Fabry-Pérot spectrometers and furthermore LADRC is used to control systems other than the PEA as well [41–46]. Possible research ventures for a synchronized LADRC would be synchronized attitude control of multiple drones for example. Seeing the ease and success that the LADRC was implemented, indicates that it should be used more widely in the industry. This research has also demonstrated the success of the more obscure parameter estimation technique, Taguchi's method, which should also be used more widely in the field of control systems engineering to determine the control parameters due to its effectiveness. This research will hopefully increase the popularity of LADRC and Taguchi's method in the field of control systems engineering.

Bibliography

[1] P. I. (PI), *PZ254E P-753 Positioning Systems User Manual*, Physik Instrumente (PI).

[2] R. Orszulik and J. Shan, "An Integral-Based Approach to the Synchronization of Multiple Piezoelectric Actuators," York University, Tech. Rep., 11 2016.

[3] W. Weng, F. Yang, and A. Z. Elsherbeni, "Linear Antenna Array Synthesis Using Taguchi's Method: A Novel Optimization Technique in Electromagnetics," *IEEE Transactions on Antennas and Propagation*, vol. 55, no. 3, pp. 723–730, March 2007.

[4] G. Tian and Z. Gao, "Frequency Response Analysis of Active Disturbance Rejection Based Control System," in *2007 IEEE International Conference on Control Applications*, Singapore, Oct 2007, pp. 1595–1599.

[5] Z. Chi and Q. Xu, "Recent Advances in the Control of Piezoelectric Actuators," *International Journal of Advanced Robotic Systems*, vol. 11, no. 11, p. 182, 2014.

[6] S. Sherrit, "Smart material/actuator needs in extreme environments in space," in *Proceedings of SPIE Smart Structures Conference*, vol. 5761, San Diego, CA, Mar 2005.

[7] R. Orszulik and J. Shan, "Integral plus double integral synchronization control for multiple piezoelectric actuators," in *2015 European Control Conference (ECC)*, Linz, Austria, July 2015, pp. 1082–1087.

[8] A. A. Rader, F. F. Afagh, A. Yousefi-Koma, and D. G. Zimcik, "Optimization of Piezoelectric Actuator Configuration on a Flexible Fin for Vibration Control using

Genetic Algorithms," *Journal of Intelligent Material Systems and Structures*, vol. 18, no. 10, pp. 1015–1033, 2007.

[9] S. Devasia, E. Eleftheriou, and S. O. R. Moheimani, "A Survey of Control Issues in Nanopositioning," *IEEE Transactions on Control Systems Technology*, vol. 15, no. 5, pp. 802–823, 2007.

[10] M. G. Borgen, G. N. Washington, and G. L. Kinzel, "Design and evolution of a piezoelectrically actuated miniature swimming vehicle," *IEEE/ASME Transactions on Mechatronics*, vol. 8, no. 1, pp. 66–76, March 2003.

[11] J. Park and W. Moon, "Hysteresis compensation of piezoelectric actuators: The modified Rayleigh model," *Ultrasonics*, vol. 50, no. 3, pp. 335 – 339, 2010.

[12] R. Orszulik, "Dynamics and Control of Smart Structures for Space Applications," Ph.D. dissertation, York University, Toronto, Ontario, Canada, 2013.

[13] Y. Liu, J. Shan, and N. Qi, "Creep modeling and identification for piezoelectric actuators based on fractional-order system," *Mechatronics*, vol. 23, no. 7, pp. 840 – 847, 2013.

[14] S. Huang, K. K. Tan, and T. H. Lee, "Adaptive Sliding-Mode Control of Piezoelectric Actuators," *IEEE Transactions on Industrial Electronics*, vol. 56, no. 9, pp. 3514–3522, Sept 2009.

[15] G. Lee, K. You, T. Kang, K. J. Yoon, J. O. Lee, and J. K. Park, "Modeling and Design of H-Infinity Controller for Piezoelectric Actuator LIPCA," *Journal of Bionic Engineering*, vol. 7, no. 2, pp. 168 – 174, 2010.

[16] Z. Li and J. Shan, "LQG-based synchronization control of fabry - perot spectrometer using multiple piezoelectric actuators (PEAs)," in *2016 IEEE International Conference on Information and Automation (ICIA)*, Ningbo, China, Aug 2016, pp. 448–453.

[17] M. Voutsogiannakis, "Calibration and Flight of a Balloon-borne O2 Atmospheric Band Fabry-Perot Spectrometer," Master's thesis, York University, 2017.

[18] Z. Gao, "Scaling and Bandwidth-Parameterization Based Controller Tuning," in *Proceedings of the 2003 American Control Conference*, vol. 6, Denver, Colorado, June 2003, pp. 4989–4996.

[19] J. Han, "From PID to Active Disturbance Rejection Control," *IEEE Transactions on Industrial Electronics*, vol. 56, no. 3, pp. 900–906, 2009.

[20] Y. Huang and W. Xue, "Active disturbance rejection control: Methodology and theoretical analysis," *ISA Transactions*, vol. 53, no. 4, pp. 963 – 976, 2014.

[21] F. J. Goforth and Z. Gao, "An Active Disturbance Rejection Control solution for hysteresis compensation," in *2008 American Control Conference*, Seattle, Washington, June 2008, pp. 2202–2208.

[22] Makeximu, L. Sun, D. Li, and M. Zhu, "Active disturbance rejection control for structural vibration," in *14th International Conference on Control, Automation and Systems (ICCAS 2014)*, Seoul, South Korea, Oct 2014, pp. 402–406.

[23] Y. Xiong, Y. Chen, Z. Sun, L. Hao, and J. Dong, "Active disturbance rejection control for output force creep characteristics of ionic polymer metal composites," *Smart Materials and Structures*, vol. 23, no. 7, pp. 1–10, June 2014.

[24] J. Tatsumi and Z. Gao, "On the enhanced ADRC design with a low observer bandwidth," in *Proceedings of the 32nd Chinese Control Conference*, Xi'an, China, July 2013, pp. 297–302.

[25] R. Orszulik and J. Shan, "Output feedback integral control of piezoelectric actuators considering hysteresis," *Precision Engineering*, vol. 47, pp. 90 – 96, 2017.

[26] S. Zhao and Z. Gao, "Active disturbance rejection control for non-minimum phase systems," in *Proceedings of the 29th Chinese Control Conference*, Beijing, China, July 2010, pp. 6066–6070.

[27] C. Fu and W. Tan, "Tuning of linear ADRC with known plant information," *ISA Transactions*, vol. 65, pp. 384 – 393, 2016.

[28] Z. Li and J. Shan, "Inverse Compensation Based Synchronization Control of the Piezo-Actuated Fabry–Perot Spectrometer," *IEEE Transactions on Industrial Electronics*, vol. 64, no. 11, pp. 8588–8597, Nov 2017.

[29] K. Krishnan and G.Karpagam, "Comparison of PID Controller Tuning Techniques for a FOPDT System," *Journal of Current Engineering and Technology*, vol. 4, no. 4, pp. 2667–2670, 2014.

[30] W.-C. Weng, F. Yang, and A. Elsherbeni, "Electromagnetics and Antenna Optimization Using Taguchi's Method," *Synthesis Lectures on Computational Electromagnetics*, vol. 2, no. 1, pp. 1–94, 2007.

[31] N. J. A. Sloane. A Library of Orthogonal Arrays. [Online]. Available: http://www.neilsloane.com/oadir/

[32] K. F. Man, K. S. Tang, and S. Kwong, "Genetic algorithms: concepts and applications [in engineering design]," *IEEE Transactions on Industrial Electronics*, vol. 43, no. 5, pp. 519–534, Oct 1996.

[33] J. H. Holland, "Genetic Algorithms," *Scientific American*, vol. 267, no. 1, pp. 66–73, 1992.

[34] J. Liu, S. Vazquez, L. Wu, A. Marquez, H. Gao, and L. G. Franquelo, "Extended State Observer-Based Sliding-Mode Control for Three-Phase Power Converters," *IEEE Transactions on Industrial Electronics*, vol. 64, no. 1, pp. 22–31, Jan 2017.

[35] Özgür Yeniay and A. Beytepe, "Penalty Function Methods for Constrained Optimization with Genetic Algorithms," *Mathematical and Computational Applications*, vol. 10, no. 1, pp. 45–56, 2005.

[36] K. J. Åström and R. M. Murray, *Feedback Systems.* Princeton University Press, February 2009.

[37] J. Shan, H. . Liu, and S. Nowotny, "Synchronised trajectory-tracking control of multiple 3-DOF experimental helicopters," *IEE Proceedings - Control Theory and Applications*, vol. 152, no. 6, pp. 683–692, Nov 2005.

[38] J. Shan, "Six-degree-of-freedom synchronised adaptive learning control for spacecraft formation flying," *IET Control Theory Applications*, vol. 2, no. 10, pp. 930–949, October 2008.

[39] H.-T. Liu, J. Shan, and D. Sun, "Adaptive synchronization control of multiple spacecraft formation flying," *Journal of Dynamic Systems, Measurement and Control, Transactions of the ASME*, vol. 129, no. 3, pp. 337–342, 2006.

[40] D. A. Hall, "Review Nonlinearity in piezoelectric ceramics," *Journal of Materials Science*, vol. 36, no. 19, pp. 4575–4601, Oct 2001.

[41] C.-E. Huang, D. Li, and Y. Xue, "Active disturbance rejection control for the ALSTOM gasifier benchmark problem," *Control Engineering Practice*, vol. 21, no. 4, pp. 556 – 564, 2013.

[42] B. Sun and Z. Gao, "A DSP-based active disturbance rejection control design for a 1-kW H-bridge DC-DC power converter," *IEEE Transactions on Industrial Electronics*, vol. 52, no. 5, pp. 1271–1277, Oct 2005.

[43] H. Sira-Ramírez, C. López-Uribe, and M. Velasco-Villa, "Linear Observer-Based Active Disturbance Rejection Control of the Omnidirectional Mobile Robot," *Asian Journal of Control*, vol. 15, no. 1, pp. 51–63, 2013.

[44] Q. Zheng and Z. Gao, "On practical applications of active disturbance rejection control," in *Proceedings of the 29th Chinese Control Conference*, July 2010, pp. 6095–6100.

[45] Y. Tang, Y. Bai, C. Huang, and B. Du, "Linear active disturbance rejection-based load frequency control concerning high penetration of wind energy," *Energy Conversion and Management*, vol. 95, pp. 259 – 271, 2015.

[46] J. Zhang, J. Feng, Y. Zhou, F. Fang, and H. Yue, "Linear Active Disturbance Rejection Control of Waste Heat Recovery Systems with Organic Rankine Cycles," *Energies*, vol. 5, no. 12, pp. 5111–5125, 2012.

Appendix A

LADRC Closed Loop Transfer Function Derivation

Convert observer states to the frequency domain using Laplace transforms.

$$Z_3 = -\beta_3 \frac{Z_1 - Y}{s} \tag{A.1}$$

$$Z_2 = \frac{Z_3 - \beta_2(Z_1 - Y) + b_0 U}{s} \tag{A.2}$$

$$Z_1 = \frac{Z_2 - \beta_2(Z_1 - Y)}{s} \tag{A.3}$$

Substitute Eq. (A.1) into Eq. (A.2) and substitute the result into Eq. (A.3).

$$Z_1 = \frac{Y\beta 1 s^2 + U b_0 s + Y\beta_2 s + Y\beta_3}{\beta_1 s^2 + s^3 + \beta_2 s + \beta_3} \tag{A.4}$$

where U is the control signal, R is the input signal and Y is the output signal

$$U = \frac{k_p(R - Z_1) - k_d Z_2 - Z_3}{b0} \tag{A.5}$$

Substitute Eq. (A.1), Eq. (A.2) and Eq. (A.4) into Eq. (A.5) and solve for U while expressing the right hand side in terms of R and Y.

$$U = \frac{(\beta_1 k_p s^2 + k_p s^3 + \beta_2 k_p s + \beta_3 k_p)R}{b_0 s(\beta_1 k_d + \beta_1 s + k_d s + s^2 + \beta_2 + k_p)} - \frac{(\beta_1 k_p s^2 + \beta_2 k_d s^2 + \beta_2 k_p s + \beta_3 k_d s + \beta_3 s^2 + \beta_3 k_p)Y}{b_0 s(\beta_1 k_d + \beta_1 s + k_d s + s^2 + \beta_2 k_p)} \tag{A.6}$$

System is expressed as $U = G_c H R - G_c Y$, where H is the feedforward component and G_c is the controller. It is desired to express the equation as such, because it can be rearranged simply to express $Y = \frac{H G_c G_p}{1 + G_c G_p}$. This is desired as the sensitivity function and open loop gain are easy to express in this format. The resulting G_c and H are:

$$H = \frac{\beta_1 k_p s^2 + k_p s^3 + \beta_2 k_p s + \beta_3 k_p}{\beta_1 k_p s^2 + \beta_2 k_d s^2 + \beta_2 k_p s + \beta_3 k_d s + \beta_3 s^2 + \beta_3 k_p} \tag{A.7}$$

$$G_c = \frac{\beta_1 k_p s^2 + \beta_2 k_d s^2 + \beta_2 k_p s + \beta_3 k_d s + \beta_3 s^2 + \beta_3 k_p}{b_0 s(\beta_1 k_d + \beta_1 s + k_d s + s^2 + \beta_2 k_p)} \tag{A.8}$$